

# Impact of a human gut microbe on *Vibrio cholerae* host colonization through biofilm enhancement

Kelsey Barrasso<sup>1,2</sup>, Denise Chac<sup>3</sup>, Meti D Debela<sup>4</sup>, Catherine Geigel<sup>5</sup>, Anjali Steenhaut<sup>1</sup>, Abigail Rivera Seda<sup>1</sup>, Chelsea N Dunmire<sup>3</sup>, Jason B Harris<sup>4,6</sup>, Regina C Larocque<sup>4</sup>, Firas S Midani<sup>7</sup>, Firdausi Qadri<sup>8</sup>, Jing Yan<sup>5,9</sup>, Ana A Weil<sup>3\*</sup>, Wai-Leung Ng<sup>1,2\*</sup>

<sup>1</sup>Department of Molecular Biology and Microbiology, Tufts University School of Medicine, Boston, United States; <sup>2</sup>Program of Molecular Microbiology, Graduate School of Biomedical Sciences, Tufts University School of Medicine, Boston, United States; <sup>3</sup>Department of Medicine, University of Washington, Seattle, United States; <sup>4</sup>Division of Infectious Diseases, Massachusetts General Hospital, Boston, United States; <sup>5</sup>Department of Molecular, Cellular and Developmental Biology, Yale University, New Haven, United States; <sup>6</sup>Department of Pediatrics, Harvard Medical School, Boston, United States; <sup>7</sup>Department of Molecular Virology and Microbiology at Baylor College of Medicine, Houston, United States; <sup>8</sup>International Center for Diarrheal Disease Research, Bangladesh, Dhaka, Bangladesh; <sup>9</sup>Quantitative Biology Institute, Yale University, New Haven, United States

**\*For correspondence:**  
 anaweil@uw.edu (AAW);  
 wai-leung.ng@tufts.edu (W-LeungN)

**Competing interest:** The authors declare that no competing interests exist.

**Funding:** See page 18

**Preprinted:** 02 February 2021  
**Received:** 12 August 2021  
**Accepted:** 25 March 2022  
**Published:** 28 March 2022

**Reviewing Editor:** Melanie Blokesch, Ecole Polytechnique Fédérale de Lausanne, Switzerland

© Copyright Barrasso et al. This article is distributed under the terms of the [Creative Commons Attribution License](https://creativecommons.org/licenses/by/4.0/), which permits unrestricted use and redistribution provided that the original author and source are credited.

**Abstract** Recent studies indicate that the human intestinal microbiota could impact the outcome of infection by *Vibrio cholerae*, the etiological agent of the diarrheal disease cholera. A commensal bacterium, *Paracoccus aminovorans*, was previously identified in high abundance in stool collected from individuals infected with *V. cholerae* when compared to stool from uninfected persons. However, if and how *P. aminovorans* interacts with *V. cholerae* has not been experimentally determined; moreover, whether any association between this bacterium alters the behaviors of *V. cholerae* to affect the disease outcome is unclear. Here, we show that *P. aminovorans* and *V. cholerae* together form dual-species biofilm structure at the air–liquid interface, with previously uncharacterized novel features. Importantly, the presence of *P. aminovorans* within the murine small intestine enhances *V. cholerae* colonization in the same niche that is dependent on the *Vibrio* exopolysaccharide and other major components of mature *V. cholerae* biofilm. These studies illustrate that multi-species biofilm formation is a plausible mechanism used by a gut microbe to increase the virulence of the pathogen, and this interaction may alter outcomes in enteric infections.

## Editor's evaluation

In this work, the authors study the previously reported positive association between the presence of the gut bacterium *Paracoccus aminovorans* and *Vibrio cholerae* during infection. They describe and image dual-species biofilm formed in vitro as well as enhanced *V. cholerae* gut colonization in the presence of *P. aminovorans* in a neonatal mouse model. Collectively, the authors conclude that *P. aminovorans* enhances biofilm formation by *V. cholerae*, which could explain the increased abundance of *P. aminovorans* in persons infected with *V. cholerae* in endemic areas, and may have impacted the course of infections in humans.

## Introduction

*Vibrio cholerae* (Vc) causes an estimated 3 million infections and 120,000 deaths each year, and larger and more deadly outbreaks have increased during the last decade (Camacho et al., 2018; Luquero et al., 2016). A wide range of clinical outcomes occur in persons exposed to Vc, ranging from asymptomatic infection to severe secretory diarrhea. It is nearly certain that many behaviors of Vc in the aquatic environment and inside the host are significantly affected by the presence of other microbes (Weil and Ryan, 2018), and recent studies provide evidence that the gut microbiota may impact the severity of cholera (Alavi et al., 2020; Hsiao et al., 2014; Levade et al., 2020; Midani et al., 2018).

Several functions of the gut microbiota influence the growth or colonization of enteric pathogens, including production of antimicrobial compounds, maintenance of the intestinal barrier, regulation of the host immune response, and modulation of available nutrients (McKenney and Pamer, 2015). Gut microbes have been shown to have an important role in Vc infection in various animal models. For instance, disruption of the commensal microbiota with antibiotics is required to allow successful Vc colonization in adult rodent models. Starvation and streptomycin treatment are needed to reduce the intestinal normal flora to allow Vc infection to occur in the cecum and the entire bowel in guinea pigs (Freter, 1955). In another case, streptomycin treatment is needed to allow Vc colonization, mainly in the cecum and large intestine, of adult mice (Nygren et al., 2009). Conversely, Vc actively employs a type VI secretion system to attack host commensal microbiota to enhance colonization of the gut in infant mice (Zhao et al., 2018). Moreover, specific microbial species have a profound impact on Vc colonization. Pre-colonization with *Blautia obeum*, an anaerobic Gram-positive bacterium, in adult gnotobiotic mice decreases the Vc counts in the feces after infection. *B. obeum* is thought to produce a signaling molecule that induces Vc into a high cell-density quorum sensing state (Hsiao et al., 2014) in which virulence gene expression is repressed (Jung et al., 2015; Watve et al., 2020). Certain microbiota species reduce Vc colonization in germfree adult and suckling mice by producing the enzyme bile salt hydrolase that degrades the host-produced virulence-activating compound taurocholate (Alavi et al., 2020; Hsiao et al., 2014). Through metabolizing host glycans into short-chain fatty acids that suppress Vc growth, a prominent commensal species, *Bacteroides vulgatus*, reduces Vc proliferation within the intestine of germfree adult mice and typical laboratory infant mice (You et al., 2019).

While the above studies exemplify how a single microbe or a group of microbes can protect the host from Vc infection, the mechanisms used by certain gut microbes to promote Vc virulence, thereby increasing the likelihood of individuals developing cholera and worsening disease outcomes, are less well understood. We have previously studied household contacts of cholera patients to understand how gut microbes impact on susceptibility to cholera, and we identified bacteria associated with increased or decreased susceptibility to Vc infection (Levade et al., 2020; Midani et al., 2018). We also observed that the gut microbial species *Paracoccus aminovorans* (Pa) was more abundant in the gut microbiota during Vc infection (Midani et al., 2018). This association between Pa and Vc is unusual because most of the native gut microbiota is typically displaced by secretory diarrhea during cholera (Hsiao et al., 2014; David et al., 2015). To determine the underlying mechanisms driving these correlative clinical findings, we evaluated the relationship between Pa and Vc in co-culture and determined the effects of Pa on Vc infection outcomes with in vivo models. Here, we show that Pa interacts directly with Vc to form dual-species biofilm structures with previously uncharacterized features. Moreover, Vc colonization inside the animal host is enhanced by the presence of Pa in the small intestine, and this effect is dependent upon Vc biofilm production. Our findings demonstrate a plausible mechanism by which a gut microbe specifically associates with Vc, and this reinforces our microbiome analysis in humans that identified Pa as highly associated with infected individuals. Our findings also demonstrate that interactions between these two species have the potential to directly impact Vc pathogenesis and alter outcomes in human Vc infection.

## Results

### ***P. aminovorans* is differentially abundant in individuals with active *V. cholerae* infection**

*Paracoccus* is a genus of soil microbes found in low abundance in the gut microbiome of humans (Yatsunencko et al., 2012; Urakami et al., 1990). Our previously published analysis of stool gut

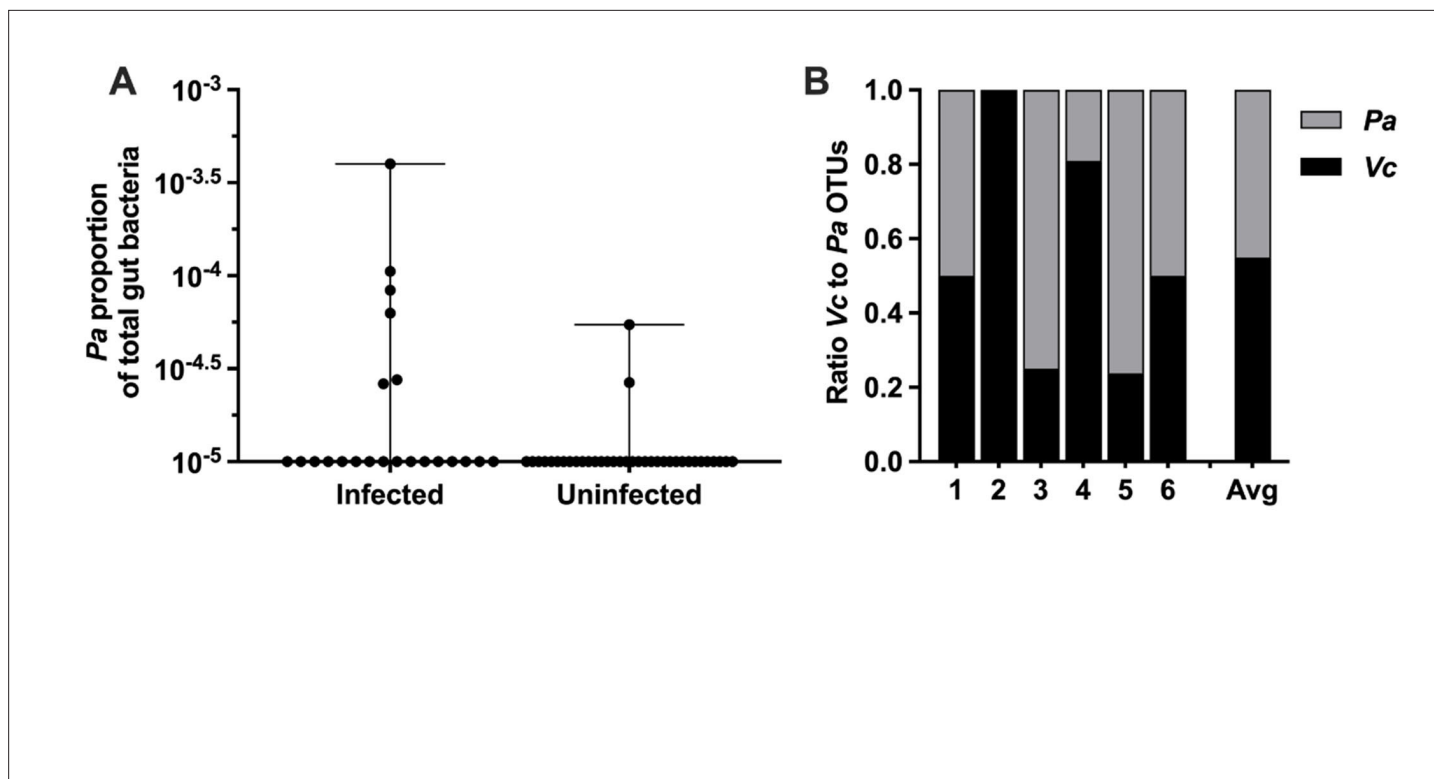


**Figure 1.** *Paracoccus aminovorans* (*Pa*) is more abundant in persons with *Vibrio cholerae* (*Vc*) infection compared to uninfected persons. In a prior study of household contacts of cholera patients in Bangladesh (*Midani et al., 2018*), *Pa* was identified as differentially abundant using a support vector machine model with recursive feature elimination in order to discriminate patterns of microbial taxa relative abundance that distinguished infected from uninfected persons. The microbiota was assessed using 16S rRNA in rectal swabs collected from individuals with *Vc* infection ( $n = 22$ ) compared to uninfected individuals ( $n = 36$ ). In this study, total sum normalization was applied to operational taxonomic unit (OTU) counts from each sample, and a median of 37,958 mapped reads per sample was generated (*Midani et al., 2018*). Based on this sequencing data, the estimated limit of detection for a *Pa* OTU is  $2.0 \times 10^{-5}$ . Raw and normalized counts of *Pa* and *Vc* are shown in **Supplementary file 1**. **(A)** Normalized relative abundance of *Pa* in infected and uninfected individuals, comparison between infected and uninfected  $p=0.009$  (Mann–Whitney nonparametric *U*-test). All data points are shown, and bars mark the maximum and minimum values. **(B)** Ratio of *Vc* to *Pa* in six *Vc*-infected persons.

The online version of this article includes the following source data for figure 1:

**Source data 1.** *Paracoccus aminovorans* (*Pa*) abundance in persons with and without *Vibrio cholerae* (*Vc*) infection.

**Source data 2.** Ratio of *Paracoccus aminovorans* (*Pa*) to *Vibrio cholerae* (*Vc*) in infected persons.

microbes from household contacts of cholera patients identified *Pa* as an unexpectedly abundant gut microbe during active *Vc* infection, and this organism was rarely found in uninfected participants (*Midani et al., 2018*). In this prior study, we used a support vector machine (SVM) model with recursive feature elimination to learn patterns of relative abundance of operational taxonomic units (OTUs) that distinguished infected (defined as *Vc* DNA detected in stool or a stool culture with *Vc* growth) from uninfected persons (*Vc* DNA undetected in stool and *Vc* stool culture negative). The model was trained on a subset of study participants and tested on another subset in a hold-out validation. Here, we have extracted data from this prior study to examine separately the *Pa* OTUs in infected compared to uninfected persons. *Pa* abundance was significantly higher as a proportion of the total sequencing reads in the stool of infected household contacts (6/22, 27%) compared to only 5.6% (2/36) of uninfected individuals (**Figure 1A**,  $p=0.009$  by Mann–Whitney *U*-test). The ratio of *Pa* to *Vc* abundance present during infection was variable and averaged 1:1 (**Figure 1B**). These findings were particularly interesting because typically there is a drastic reduction of nearly all gut microbes during active *Vc* infection (*Hsiao et al., 2014; David et al., 2015*) due to secretory diarrhea, oral rehydration solution ingestion, and *Vc* infection itself, and yet here *Pa* was found in an increased abundance in some actively infected participants. The *Vc* count in *Pa*-colonized infected household contacts compared to non-*Pa* colonized household contacts was modestly higher (approximately threefold) in this study;

however, statistically the difference was not significant (Mann–Whitney *U*-test,  $p=0.1474$ ), which is likely due to small sample size (**Supplementary file 1**). Based on these findings, we hypothesized that *Pa* may be resistant to displacement from the gut during infection. While our previous study demonstrates a positive correlation between *Pa* in human stool and *Vc* infection, a causal relationship between this gut microbiota species and *Vc* infection had not been previously established.

### ***Pa* increases *Vc* host colonization**

We modified a well-established infant mouse colonization model (*Klose, 2000*) to assess whether the presence of *Pa* in the small intestine would promote *Vc* host colonization. First, we isolated a spontaneous streptomycin-resistant (Strep<sup>R</sup>) mutant derived from the ATCC-type strain of *Pa* for selection and enumeration of *Pa* following host colonization. Infant mice (3-day-old) were intragastrically inoculated with *Pa* ( $10^7$  colony-forming units [CFUs]) every 12 hr for four doses (0, 12, 24, and 36 hr). At 24 hr (i.e., 12 hr after the second *Pa* inoculation and right before the third *Pa* inoculation) and 48 hr (i.e., 12 hr after the last *Pa* inoculation), small intestines from these animals were dissected and homogenized. Gut homogenates were serially diluted and plated on medium containing streptomycin to assess *Pa* colonization. Strep<sup>R</sup> *Pa* colonies ( $>10^6$  CFUs/small intestine) were recovered at these two time points (**Figure 2A**), and no Strep<sup>R</sup> colonies were detected in the mock-treated group, indicating that *Pa* successfully and stably colonized the small intestines of these animals using these methods at least for 12 hr. Unlike previous studies (*Freter, 1955; Nygren et al., 2009*), pretreatment with antibiotics was not required for *Pa* colonization (**Figure 2A**). Sequencing analysis of the mouse small intestines demonstrated no significant change in the microbial composition and diversity with and without *Pa* colonization (**Figure 2—figure supplement 1**).

We then evaluated if pre-colonization by *Pa* would influence *Vc* colonization in the small intestine. Four doses of *Pa* were inoculated into infant mice as described above. Negative control animals were inoculated with sterile media in place of *Pa* over the same dosing schedule. 12 hr after the last *Pa* inoculation (i.e., 48 hr after the first *Pa* inoculation), these animals were infected with *Vc* ( $10^6$  CFU) to evaluate whether pre-colonization with *Pa* had an impact on *Vc* colonization. Although we do not fully understand the exact composition and growth dynamics of *Vc* and *Pa* inside the human gut, the pre-colonization/infection scheme was aimed to closely simulate the ratio of *Pa* to *Vc* observed in the gut microbiota of *Vc*-infected humans (**Figures 1 and 2A**). Comparing *Pa* pre-colonized mice to the control group, there was a significant increase ( $\sim 10$ -fold,  $p \leq 0.0001$ ) of *Vc* colonization in the mice pre-colonized with *Pa* (**Figure 2B**) 24 hr after infection. This enhanced intestinal colonization by *Vc* in the *Pa*-colonized mice was observed as early as 6 hr after infection and maintained throughout the colonization period (**Figure 2—figure supplement 2**). We did not monitor *Vc* counts in the small intestine beyond 24 hr after infection due to institutional restrictions. Using this infection model, similar to human infection, the *Vc:Pa* ratio inside the mouse intestine at the early stage of infection (6 hr after *Vc* infection, 18 hr after the last *Pa* inoculation) was variable, but was approximately 10:1 (**Figure 2—figure supplement 2**). We noticed that once *Pa* inoculation ended *Pa* abundance in the small intestine decreased over time but was still detectable 22 hr after the last inoculation (i.e., 10 hr after *Vc* infection; **Figure 2—figure supplement 2**). Thus, even though this animal model does not fully mimic *Vc* infection of human host, it allows a sufficient time to study the interaction between *Vc* and *Pa* in the intestinal environment.

We reasoned that it was also possible for *Vc* and *Pa* to encounter one another in the environment before entering the host. To model this scenario, *Vc* was mixed with *Pa* in a 1:1 ratio, and the mixture was used immediately for animal infection. In agreement with the results obtained with the *Pa* pre-colonization model, *Vc* intestinal colonization was significantly higher when coinfecting with *Pa* than without *Pa* (**Figure 2C**). Given that *Pa* colonization did not overtly change the overall composition of the gut microbiota (**Figure 2—figure supplement 1**), collectively, our results demonstrate that the presence of a single gut microbiota species is sufficient to increase *Vc* host colonization. Our findings also illustrate that our approach to microbiome studies in humans (*Levade et al., 2020; Midani et al., 2018*) can be used as a predictive tool to identify gut microbes that alter *Vc* colonization.

### ***Pa* promotes *Vc* biofilm formation**

To investigate if the increased *Vc* intestinal colonization is due to direct interactions between *Vc* and *Pa*, these two species were co-cultured and allowed to propagate for 3 days where both planktonic

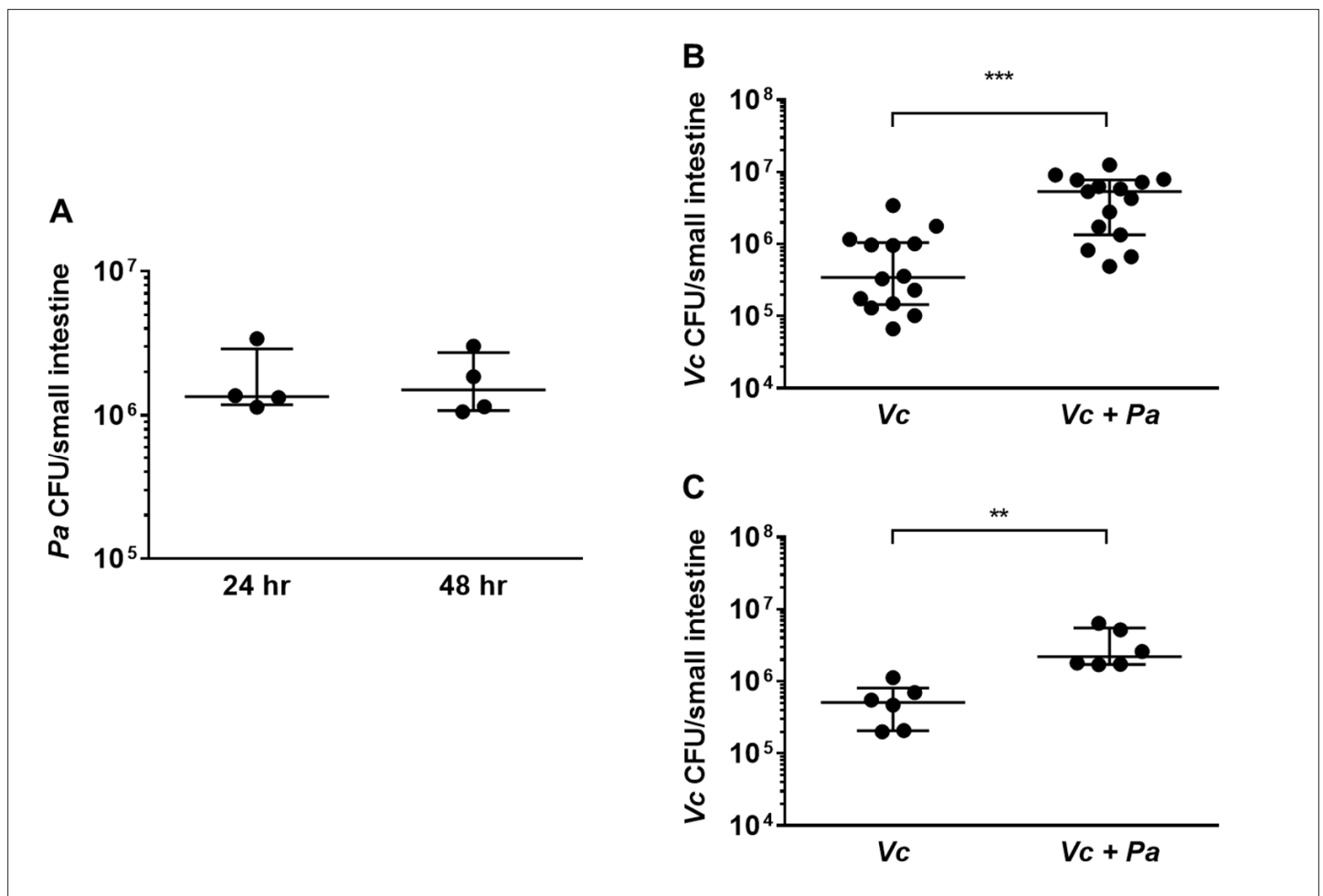


**Figure 2.** The presence of *Paracoccus aminovorans* (*Pa*) enhances *Vibrio cholerae* (*Vc*) colonization in the infant mouse intestine. **(A)** 3-day-old infant mice were intragastrically inoculated with  $10^7$  colony-forming unit (CFU) of *Pa* every 12 hr twice or four times. 12 hr after the second or fourth dose of *Pa* inoculation (i.e., at 24 hr and 48 hr, respectively), mice were sacrificed and CFUs were enumerated by plating serial dilutions of small intestine samples on selective media. **(B)** 3-day-old infant mice were intragastrically inoculated four times with LB or  $10^7$  CFU of *Pa* for every 12 hr, and 12 hr after the last *Pa* inoculation, the animals were infected with  $10^6$  CFU of WT *Vc*. Mice were sacrificed 20–24 hr post infection, and the small intestine samples were taken to enumerate *Vc*. Bars on graphs depict median value with 95% confidence interval (CI) and individual data points plotted. Unpaired nonparametric *U*-test (Mann–Whitney); \*\*\* $p < 0.001$ . **(C)** *Vc* was inoculated intragastrically into the animals alone or together with *Pa* in a 1:1 ratio. After 24 hr, enumeration of *Vc* was performed as described above. Unpaired nonparametric *U*-test (Mann–Whitney); \*\* $p < 0.01$ .

The online version of this article includes the following source data and figure supplement(s) for figure 2:

**Source data 1.** Viable cell count of *Paracoccus aminovorans* (*Pa*) in infant mouse intestine.

**Source data 2.** Viable cell count of *Vibrio cholerae* (*Vc*) in the infant mouse intestine with and without *Pa* pre-colonization.

**Source data 3.** Viable cell count of *Vibrio cholerae* (*Vc*) in the infant mouse intestine with and without *Pa* co-infection.

**Figure supplement 1.** *Paracoccus aminovorans* (*Pa*) colonization does not significantly alter the mouse gut microbial diversity.

**Figure supplement 1—source data 1.** Abundance of microbes in the mouse intestine with and without *Pa* colonization.

**Figure supplement 1—source data 2.** Principal Component Analysis of microbial abundance in mouse intestine with and without *Pa* colonization.

**Figure supplement 2.** *Paracoccus aminovorans* (*Pa*) colonization significantly increases *Vibrio cholerae* (*Vc*) small intestine colonization.

**Figure supplement 2—source data 1.** Viable cell count of *Vibrio cholerae* (*Vc*) in the mouse small intestine with and without *Pa* pre-colonization.

**Figure supplement 2—source data 2.** Viable cell count of *Paracoccus aminovorans* (*Pa*) and *Vibrio cholerae* (*Vc*) in the mouse small intestine 6 hours after *Vc* infection.

**Figure supplement 2—source data 3.** Viable cell count of *Paracoccus aminovorans* (*Pa*) in the mouse intestine with and without *Vibrio cholerae* (*Vc*) infection.

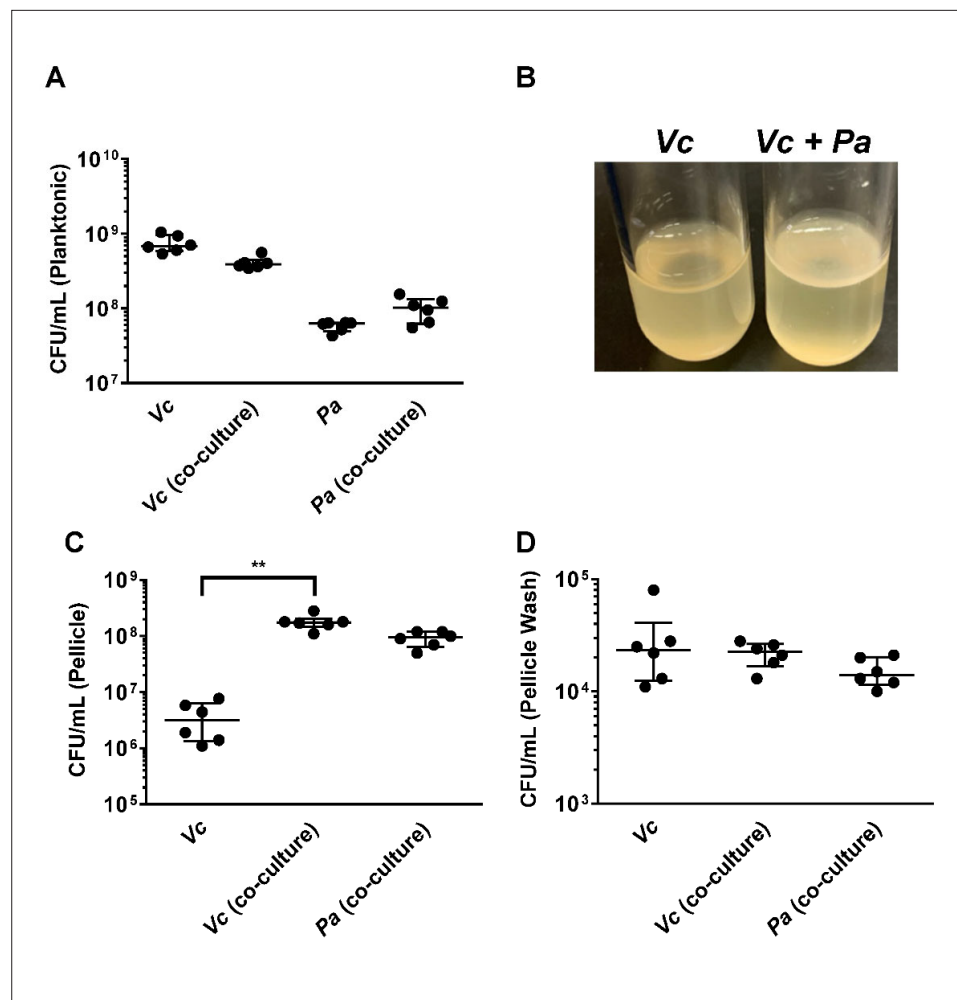


**Figure 3.** *Paracoccus aminovorans* (*Pa*) promotes biofilm formation of *Vibrio cholerae* (*Vc*). **(A)** Planktonic cell counts from cultures used for pellicle analysis of *Vc* and *Pa* grown together or in monoculture. **(B)** Representative images of pellicles formed by *Vc* grown in monoculture and co-culture with *Pa*. Colony-forming unit (CFU) counts of each strain in **(C)** pellicle samples and **(D)** spent medium used to wash the pellicle. Bars on graphs depict median value with 95% confidence interval (CI) and individual data points plotted. Unpaired nonparametric *U*-test (Mann–Whitney): \*\* $p \leq 0.01$ .

The online version of this article includes the following source data and figure supplement(s) for figure 3:

**Source data 1.** Viable cell count in for *Paracoccus aminovorans* (*Pa*) and *Vibrio cholerae* (*Vc*) in the planktonic phase in mono- and co-cultures.

**Source data 2.** Pellicle formation in *Vc* mono- and *Vc/Pa* coculture.

**Source data 3.** Viable cell count in for *Paracoccus aminovorans* (*Pa*) and *Vibrio cholerae* (*Vc*) in the pellicle formed by mono- and co-cultures.

**Source data 4.** Viable cell count in for *Paracoccus aminovorans* (*Pa*) and *Vibrio cholerae* (*Vc*) released by washing of the pellicle formed by mono- and co-cultures.

**Figure supplement 1.** *Paracoccus aminovorans* (*Pa*) cultures increase biofilm production in *Vibrio cholerae* (*Vc*).

**Figure supplement 1—source data 1.** Crystal violet assays of biofilm formed by *Vc* mono- and *Vc/Pa* co-cultures.

**Figure supplement 1—source data 2.** Crystal violet assays of biofilm formed by *Vc* mono- and *Vc/Pa* co-cultures using *vpsL* mutants with and without complementation plasmids.

**Figure supplement 1—source data 3.** Viable cell count of of pellicles formed by *Vc* mono- and *Vc/Pa* co-cultures using *vpsL* mutants with and without complementation plasmids.



growth and pellicle formation (i.e., biofilm formation at the air–liquid interface) of both species were monitored. There was a small difference (less than twofold) in growth in the planktonic phase of either Vc or Pa in the co-cultures when compared to the cultures containing a single species (**Figure 3A**). However, more importantly, the Vc/Pa co-culture formed a pellicle that was visibly thicker and more robust than that formed by Vc monoculture (**Figure 3B**). The Pa monoculture did not form a visible pellicle. The co-culture pellicle samples were carefully lifted and removed from the culture medium, washed, and agitated to release single cells for enumeration of each species. Compared to Vc monoculture, the co-culture samples contained over 50-fold more Vc cells while the ratio of Vc to Pa approached approximately 1:1 (**Figure 3C**). Moreover, only a small fraction (0.01%) of Vc and Pa

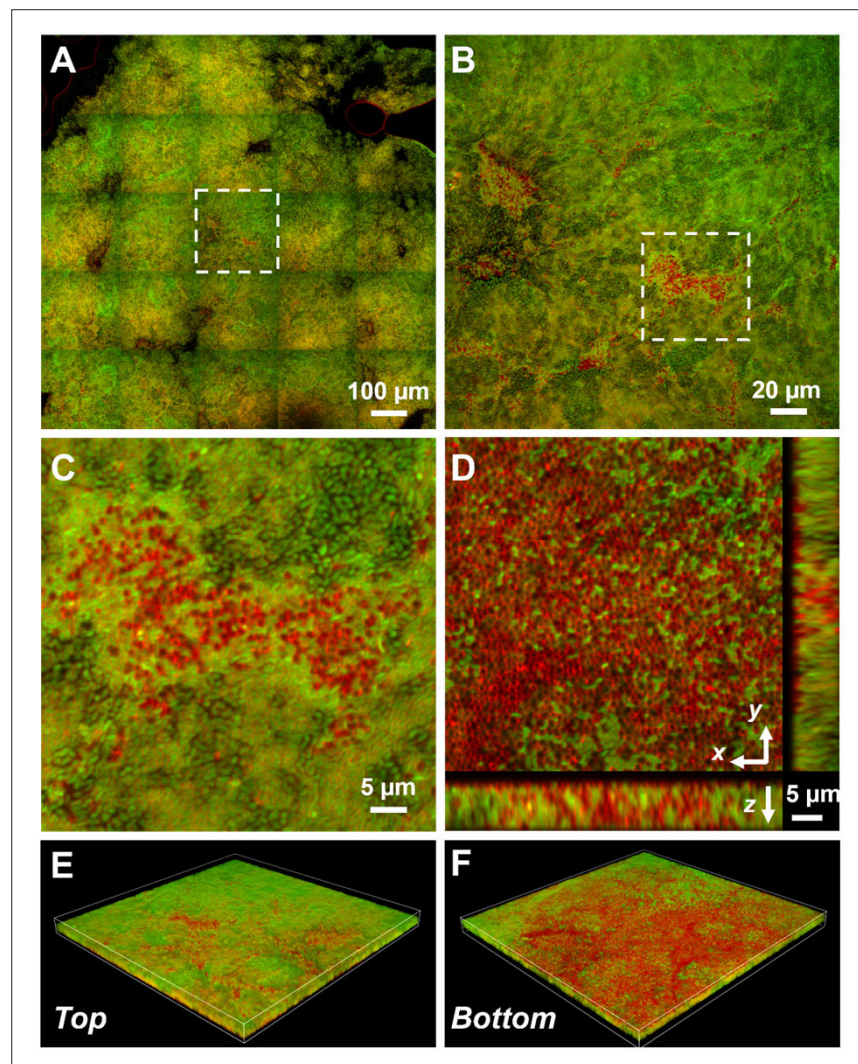


**Figure 4.** Representative microscopy images of *Vibrio cholerae* (Vc) and *Paracoccus aminovorans* (Pa) dual-species pellicles. (A) Large-scale cross-sectional image of the internal structure in a co-culture pellicle. All cells are stained with FM 4-64 and Vc cells constitutively express mNeonGreen. Therefore, the red signal in the overlay image corresponds primarily to Pa cells. The Pa cells can also be distinguished from Vc cells by their characteristic cocci shape. (B) Zoom-in view of the region highlighted in (A). (C) Zoom-in view of the region highlighted in (B). (D) Cross-sectional views of the region shown in (C), at the bottom of the pellicle. Pa cells exist mainly at the pellicle–liquid interface, with clusters of Pa cells penetrating into the interior of the pellicle. (E, F) Top (E) and bottom (F) views of the co-culture structure shown in (B), rendered in 3D.

The online version of this article includes the following figure supplement(s) for figure 4:

**Figure supplement 1.** Negative controls for wheat germ agglutinin (WGA) staining and the reporter strain.

could be washed off from the isolated pellicles (**Figure 3D**), suggesting that these species are tightly integrated into the pellicle.

Based on the above data, we hypothesize that Vc and Pa form dual-species biofilms at the air–liquid interface. This is unexpected because Vc is known to form a clonal community in both in vitro and in vivo biofilms and these are known to exclude other species, including even planktonic Vc cells (**Millet, 2014; Nadell et al., 2015**). To test this hypothesis, we transferred the co-culture pellicles onto coverslips for imaging with confocal microscopy (**Figure 4**). All cells in the pellicle were stained with FM 4-64 membrane dye, and Vc cells were differentiated from Pa using a constitutively produced mNeonGreen reporter (**Shaner et al., 2013**) expressed from a neutral Vc locus (**Dalia et al., 2014**). Pa cells have a cocci morphology that is distinct from the characteristic Vc curved-rod shape. In the Vc/Pa co-culture pellicles, we observed a continuous film structure spanning the entire pellicle (**Figure 4A**). Notably, cocci-shaped Pa cells were clearly visible in the co-culture pellicle (**Figure 4B and C**), consistent with the CFU quantification in **Figure 3A**. Interestingly, Pa cells were found throughout the pellicle, with a higher abundance in the bottom layer (**Figure 4D–F**) and in close association with Vc cells. In summary, we found that Vc and Pa coexist stably in the pellicle structure and this relationship may explain the mechanism by which Pa resists displacement in humans during active Vc infection.

Next, we used a standard crystal violet (CV) microtiter plate assay (**O’Toole, 2011**) to quantitatively evaluate how Vc and Pa interact under pellicle-forming conditions. Vc and Pa were simultaneously inoculated into the wells of microplates in two different Vc:Pa ratios (1:1 and 1:10). We also tested if the viability of Pa was crucial for this interaction by using heat-killed Pa as a control. Consistent with our pellicle compositional analysis, Vc formed a more robust biofilm than Pa under these conditions as demonstrated by increased CV staining in wells containing Vc only compared to wells containing Pa only (**Figure 5A**). Importantly, CV staining was increased in wells containing Vc and live Pa compared to wells with Vc only in a concentration-dependent manner (**Figure 5A**). In contrast, CV staining was not different in wells containing Vc and heat-killed Pa compared to wells with Vc only (**Figure 5A**).

To replicate our mouse experiments (**Figure 2**), we also tested if the order in which the two species encounter one another is critical for the Vc biofilm enhancement phenotype. Pa was grown in wells 24 hr before the addition of Vc. As in our previous results in the co-inoculation experiment, an increase in CV staining was observed in wells in which the two species were added sequentially, but not in the wells with Vc only (**Figure 3—figure supplement 1**). Moreover, wells pre-incubated with heat-killed Pa and subsequently inoculated with Vc had no increase in CV staining compared to wells inoculated with Vc alone (**Figure 3—figure supplement 1**). Together, our biofilm quantification data suggest that the presence of Pa, regardless of the order of encounter, results in an enhanced biofilm formation of Vc.

### **Vibrio exopolysaccharide is essential for a stable biofilm structure formed by Vc and Pa**

To understand what biofilm component is required for the enhancement of biofilm production in Vc/Pa co-culture, we repeated the above experiments with a  $\Delta vpsL$  Vc mutant that cannot produce the *Vibrio* exopolysaccharide (VPS) necessary for mature biofilm formation (**Yildiz and Schoolnik, 1999**). In contrast to our observations in culture of a  $vpsL^+$  strain, there was no significant increase in CV staining in wells with  $\Delta vpsL$  mutant and Pa co-culture when compared to wells with the  $\Delta vpsL$  mutants only (**Figure 5B**). The biofilm formation defects of the Vc  $\Delta vpsL$  mutants and the increased biofilm formation response in the presence of Pa could be restored by the introduction of a plasmid constitutively expressing *vpsL* (**Figure 3—figure supplement 1**).

We then tested if the presence of Pa changes *vps* gene expression in Vc as one of the mechanisms responsible for enhanced biofilm formation. Vc monoculture and Vc/Pa co-culture were grown statically to induce pellicle formation, and cells near the air–liquid interface where pellicle was formed were collected. Using qRT-PCR, we determined that the relative transcript levels of *vpsL* (the first and a representative gene in the *vpsII* operon in Vc) were significantly higher in the Vc/Pa co-culture than that in the Vc monoculture after 24–48 hr of growth (**Figure 5C**). There was no significant difference in *vpsL* transcript levels after 72 hr of co-culture. Our results suggest that Pa induces Vc biofilm gene expression when the two species are cultured together, especially at the early stage of interaction, creating the conditions for increased pellicle formation in co-cultures.



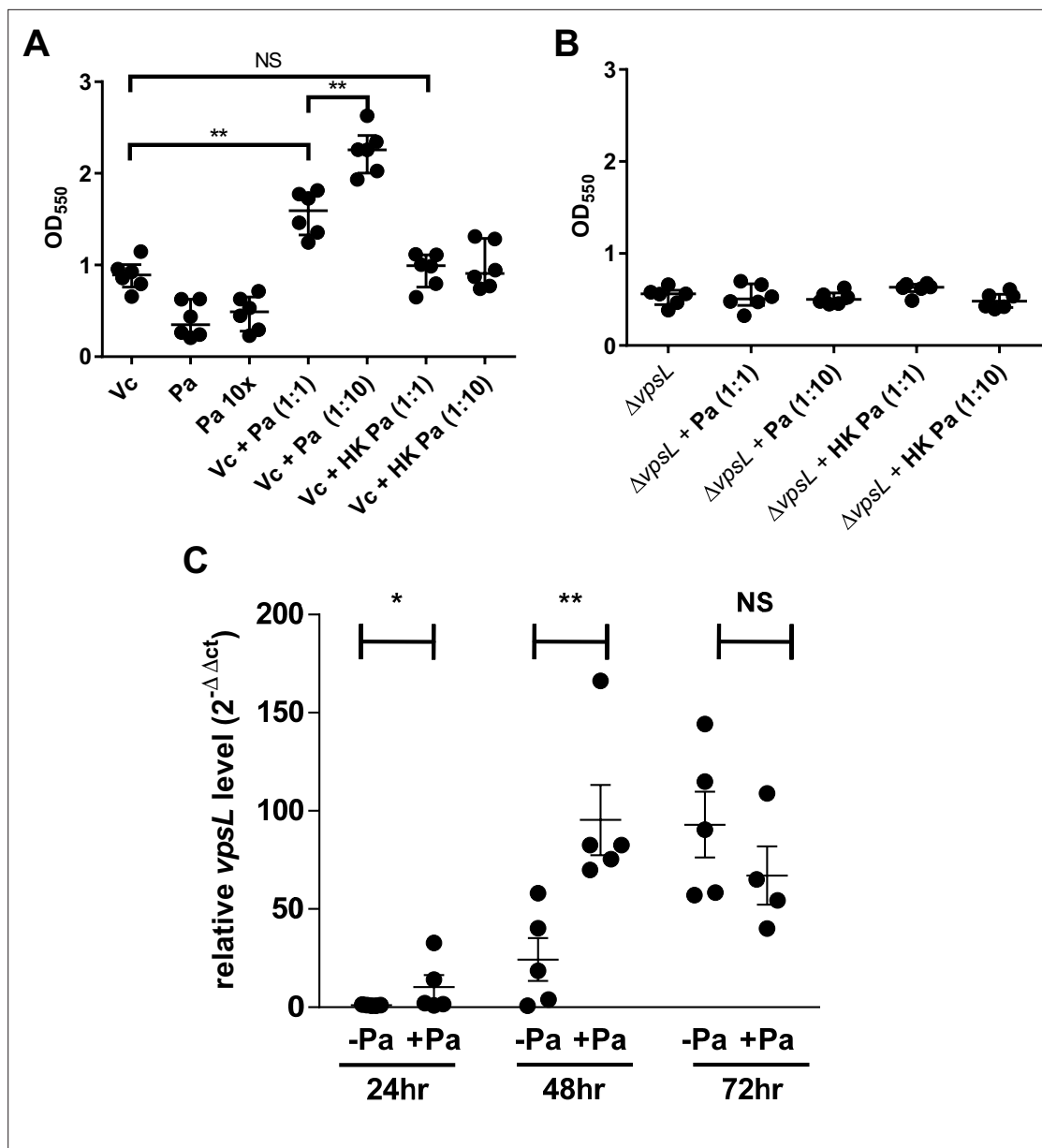


**Figure 5.** *Paracoccus aminovorans* (*Pa*) increases biofilm production in *Vibrio cholerae* (*Vc*). Crystal violet assays were performed in 96-well microtiter plates to quantify biofilm formation. Overnight-grown (A) wild-type *Vc* or (B)  $\Delta vpsL$  mutant and *Pa* cultures were diluted to a final concentration of  $10^6$  colony-forming unit (CFU) in a total volume of 200  $\mu$ L/well. In samples containing a 1:10 ratio of *Vc/Pa*, *Pa* was diluted to a final concentration of  $10^7$  CFU. Samples with heat-killed (HK) *Pa* are specified on the x-axis. Microtiter plates were incubated at 37°C for 24 hr. Crystal violet staining and ethanol solubilization were performed as previously described (O'Toole, 2011). Absorbance of the crystal violet stain was measured at 550 nm using a BioTek Synergy HTX plate reader. Data are represented with horizontal lines indicating the mean with standard deviation. Unpaired *U*-test (Mann–Whitney); \*\* $p < 0.01$ . (C) *Vc* and *Pa* were co-cultured at a 1:10 ratio statically for 72 hr at 30°C. At the specified time points, culture from the air–liquid interface was sampled and the RNA extracted. Relative *vpsL* transcript levels were determined by qRT-PCR using housekeeping gene *groEL* and the  $\Delta\Delta CT$  analytic method. Bars on graphs depict mean with standard error of mean (SEM). Mann–Whitney *U*-test was performed, \*\* $p < 0.01$ , \* $p < 0.05$ , NS  $p > 0.05$ .

The online version of this article includes the following source data for figure 5:

**Source data 1.** Crystal violet assays of biofilm formed by *Vc* mono- and *Vc/Pa* co-cultures using WT with live or heat-killed *Pa*.

**Source data 2.** Crystal violet staining of biofilm formed by *Vc* mono- and *Vc/Pa* co-cultures using *vpsL* mutants with live and heat-killed *Pa*.

**Source data 3.** qRT-PCR analysis of *vpsL* gene in cells in biofilm formed by *Vc* mono- and *Vc/Pa* co-cultures.

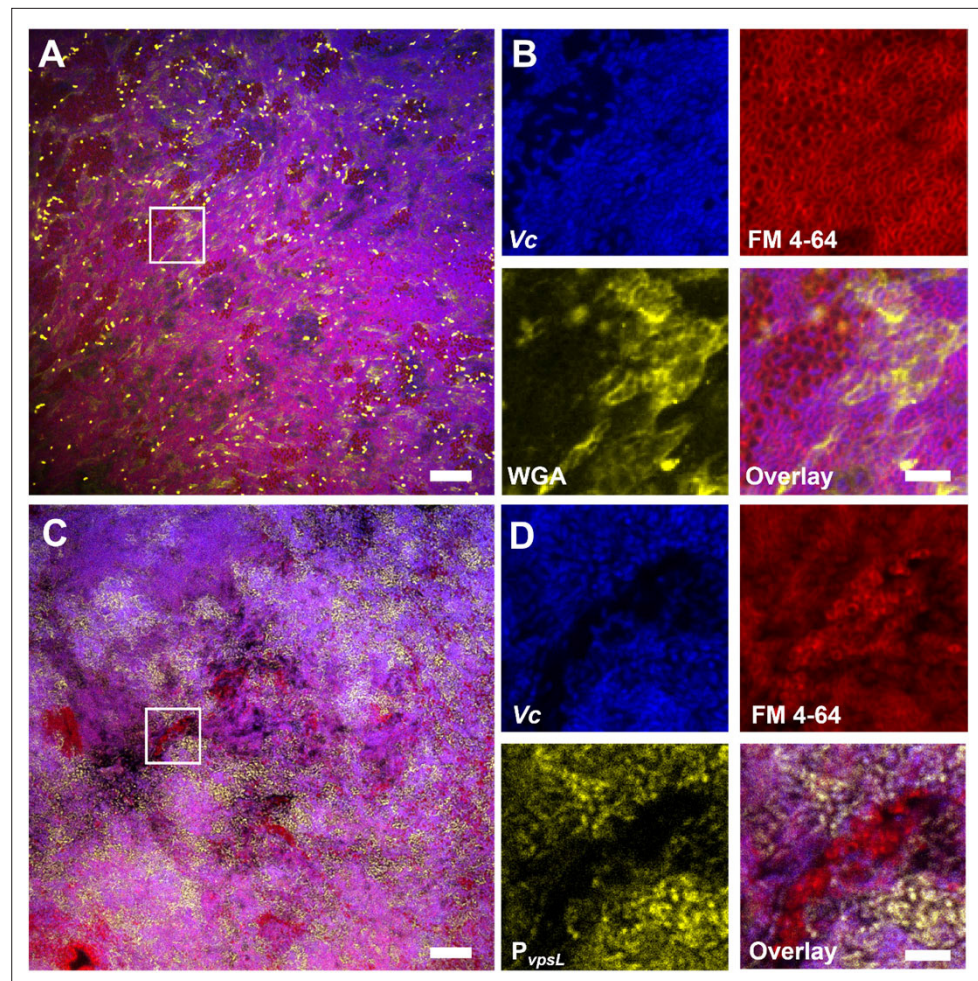


**Figure 6.** *Vibrio cholerae/Paracoccus aminovorans* (Vc/*Pa*) co-culture biofilms depend on *Vibrio* exopolysaccharide (VPS). **(A)** Representative cross-sectional view of the bottom layer of a co-culture pellicle with wheat germ agglutinin (WGA) staining. Vc cells constitutively express SCFP3A cytosolically; all cells were stained with FM 4-64 membrane stain; WGA is conjugated to Oregon Green and shown in yellow. Note that WGA also stained dead cells with an exposed peptidoglycan layer, corresponding to the bright spots in the image. Scale bar: 20  $\mu$ m. **(B)** Zoom-in view of the region highlighted by the white box in **(A)**. Shown are separate channels from Vc cell fluorescence (SCFP3A, blue), membrane staining (FM 4-64, red), WGA staining (Oregon Green, yellow), and the overlay of the three channels. *Pa* cells can be distinguished from Vc cells by both the absence of SCFP3A fluorescence and the distinct cell shape. Scale bar: 5  $\mu$ m. **(C)** Representative cross-sectional view of a co-culture pellicle in which the Vc cells harbor a  $P_{vpsL}$ -mNeonGreen reporter. Scale bar: 20  $\mu$ m. **(D)** Zoom-in view of the region highlighted by the white box in **(C)**. Shown are separate channels from Vc cell fluorescence (SCFP3A, blue), membrane staining (FM 4-64, red), *vpsL* reporter (mNeonGreen, yellow), and the overlay of the three channels. Scale bar: 5  $\mu$ m.

To further investigate the role of VPS in promoting co-culture biofilms, we stained the co-culture pellicle in situ with wheat germ agglutinin (WGA), a common stain for the N-acetylglucosamine (GlcNAc) moieties that is a component of VPS (Yildiz *et al.*, 2014). Note that for Gram-negative bacteria, including Vc and *Pa*, the WGA lectin molecules do not pass through the outer membrane of healthy cells. Indeed, control experiments show that healthy *Pa* cells and Vc  $\Delta vpsL$  mutant cells do not show positive VPS staining (Figure 4—figure supplement 1). To avoid spatial overlap with the membrane stain (excited at 561 nm), the Vc cells used in this experiment express a cyan-fluorescent protein SCFP3A cytosolically (excited at 445 nm), and the WGA is conjugated to Oregon Green (excited at 488 nm). Figure 6A shows a Vc/*Pa* co-culture pellicle, in which extensive WGA signal is observed. Zoom-in of the pellicle shows the characteristic envelope structures around clusters of Vc cells (Figure 6B), consistent with the known VPS staining pattern in submerged Vc biofilms

(Berk et al., 2012). We also noticed that regions with strong VPS signal are not necessarily spatially correlated with clusters of *Pa* cells.

Next, to demonstrate that co-culturing with *Pa* increases *vps* gene expression, we used a Vc strain harboring a  $P_{vpsL}$ -*mNeonGreen* reporter and repeated the imaging of the co-cultured pellicle. **Figure 6C** shows that in the co-cultured pellicle *vpsL* expression is elevated in subpopulations of Vc cells in the co-culture. Zoom-in views show that even adjacent to *Pa* cell clusters some Vc cells have high *vpsL* expression and others have basal-level expression (**Figure 6D**, **Figure 4—figure supplement 1**). These results are consistent with the qRT-PCR results in **Figure 5C**, suggesting that *Pa* induces Vc biofilm gene expression in co-culture. Together, these results suggest that the physical presence of *Pa* in the co-culture pellicle augments the production of VPS in Vc cells, leading to increased Vc biofilm formation; the *Pa* cells, in turn, require VPS to be integrated into the 3D structure of the pellicle.

## Enhancement of Vc host colonization by *Pa* depends on biofilm exopolysaccharide

Biofilm-grown Vc cells are known to be more infectious in humans due to increased resistance to gastric pH and higher expression of virulence factors (e.g., such as the toxin co-regulated pilus, which mediates host colonization) compared to planktonically grown cells (Tamayo et al., 2010; Gallego-Hernandez et al., 2020; Zhu and Mekalanos, 2003). We hypothesize that because Vc biofilm formation is enhanced in the presence of *Pa* this results in increased virulence inside the host in a VPS-dependent manner. Previous studies report that Vc El Tor biotype strains require certain growth conditions (e.g., AKI) to induce virulence gene expression in vitro (DiRita et al., 1996; Iwanaga et al., 1986). However, these specific growth conditions include culture agitation, which would prevent proper interaction of Vc and *Pa*. Therefore, using qRT-PCR, we measured virulence gene expression in Vc/*Pa* co-culture and compared this to Vc monoculture grown statically in identical conditions to those that favor biofilm formation. As expected, *ctxA* and *tcpA* relative transcript levels were low in all samples; however, there was a modest increase in the expression of these two virulence genes in the Vc/*Pa* co-culture compared to the Vc monoculture (**Figure 7—figure supplement 1**).

To further test our hypothesis and measure if the effect of the Vc/*Pa* biofilm interaction impacts host colonization, we compared the colonization efficiency between wild-type (WT) or the  $\Delta vpsL$  mutants in infant mice with and without *Pa* pre-colonization. As shown previously (Fong et al., 2010), the  $\Delta vpsL$  mutant was able to colonize the mouse small intestine as well as the WT *vpsL*<sup>+</sup> strain, confirming that VPS is not absolutely required for host colonization when Vc was administered to the animals alone. In contrast, while *Pa* increased WT *vpsL*<sup>+</sup> Vc colonization, the  $\Delta vpsL$  mutant did not exhibit the enhanced colonization phenotype in the *Pa* pre-colonized mice (**Figure 7A**). Host colonization enhancement caused by *Pa* pre-colonization could be restored in the  $\Delta vpsL$  mutants with a plasmid constitutively expressing *vpsL*, but not with the empty vector (**Figure 7—figure supplement 2**). Similar results were observed using the co-infection model; when Vc  $\Delta vpsL$  mutants were coinfecting with *Pa*, there was no increase in host colonization (**Figure 7B**). Together, we concluded that the enhancement of Vc intestinal colonization in the presence *Pa* is dependent on the VPS, consistent with our in vitro data.

## Accessory biofilm matrix proteins are involved in *Pa* and Vc interaction

Mature Vc biofilm is stabilized with a variety of accessory matrix proteins in addition to the VPS (Berk et al., 2012; Fong et al., 2006; Fong and Yildiz, 2007). To interrogate the roles of these components in the interactions between Vc and *Pa*, we tested mutants lacking the cell-cell adhesion proteins RbmA (Berk et al., 2012; Fong et al., 2006; Absalon et al., 2011) and mutants lacking surface adhesion redundantly conferred by RbmC and Bap1 (Berk et al., 2012; Fong and Yildiz, 2007; Absalon et al., 2011) for their ability to increase biofilm formation in the presence of *Pa* using CV assays (**Figure 7C**). When compared to the wells containing the  $\Delta rbmA$  mutant alone, the CV staining was higher in the wells with the  $\Delta rbmA$  mutant co-cultured with *Pa*. However, the increase was not as high in the  $\Delta rbmA$  mutant/*Pa* co-culture compared to that in WT Vc/*Pa* co-culture (**Figure 7C**). Furthermore, the presence of *Pa* did not increase CV staining in the wells containing the  $\Delta rbmC \Delta bap1$  mutants (**Figure 7C**) because the  $\Delta rbmC \Delta bap1$  mutant is not able to adhere to the interface.

We then performed the infant mouse colonization experiments with Vc biofilm matrix protein mutants using the *Pa* co-infection model to test the roles of these proteins in vivo. For this series of experiments, each Vc biofilm mutant was coinfecting into the animals with *Pa* in 1:1 ratio. In agreement

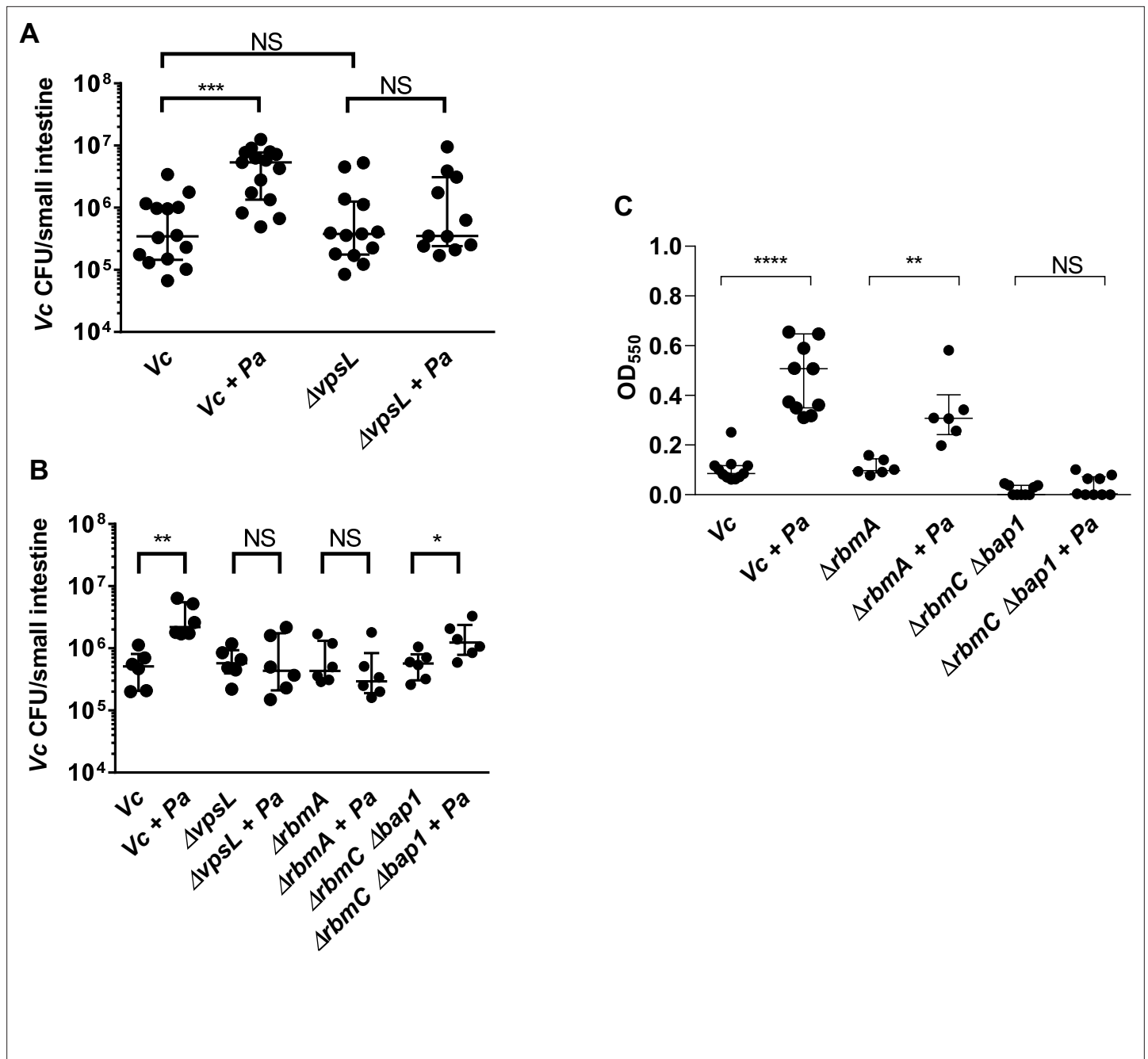


**Figure 7.** Enhanced *Vibrio cholerae* (Vc) intestinal colonization in the presence of *Paracoccus aminovorans* (Pa) is dependent on *Vibrio* exopolysaccharide (VPS) and accessory matrix proteins. **(A)** 3-day-old infant mice were intragastrically inoculated with LB or  $10^7$  colony-forming unit (CFU) of Pa every 12 hr for a period of 48 hr, and subsequently infected with  $10^6$  CFU of a Vc strain defective for extracellular matrix production ( $\Delta vpsL$ ). Mice were sacrificed 20–24 hr post infection, and small intestine samples were taken to enumerate Vc CFU. Data from infection with the wild-type Vc strain (**Figure 2B**) are shown again here for comparison purposes. **(B)** Vc WT or different biofilm mutants were mixed with Pa in 1:1 ratio, and the mixture was used immediately for animal infection. Mice were sacrificed 20–24 hr post infection, and small intestine samples were taken to enumerate Vc CFU. Each symbol represents an individual mouse. Data from infection with the WT Vc strain (**Figure 2C**) are shown again here for comparison purposes. **(C)** Crystal violet assays performed in 96-well plates to quantify pellicle formation. Overnight cultures of Vc  $\Delta rbmA$ ,  $\Delta rbmC \Delta bap1$ , and Pa were diluted in fresh LB and plated as 200  $\mu$ L/well. Samples were co-cultured in 1:10 ratios of Vc/Pa and incubated at 37°C for 24 hr. Crystal violet staining was then performed as previously described. For all panels, horizontal lines indicating median with standard deviation are shown. Unpaired Mann–Whitney U-test; \*\*\*\* $p \leq 0.0001$ , \*\*\* $p \leq 0.001$ , \*\* $p \leq 0.01$ , \* $p \leq 0.05$ , NS  $p > 0.05$ .

The online version of this article includes the following source data and figure supplement(s) for figure 7:

**Source data 1.** Viable cell count of Vc in the mouse intestine with and without Pa pre-colonization using Vc WT and vpsL mutants.

Figure 7 continued on next page



Figure 7 continued

**Source data 2.** Viable cell count of Vc in the mouse intestine with and without Pa pre-colonization using Vc WT and different biofilm matrix protein mutants.

**Source data 3.** Crystal violet staining of biofilm formed by different biofilm matrix protein mutants with and without Pa.

**Figure supplement 1.** *ctxA* and *tcpA* gene expression in *Vibrio cholerae* (Vc) monoculture and *Vibrio cholerae*-*Paracoccus aminovorans* (Vc-Pa) co-culture.

**Figure supplement 1—source data 1.** qRT-PCR analysis of virulence genes in Vc with and without Pa.

**Figure supplement 2.** Complementation of *vpsL* mutant in vivo.

**Figure supplement 2—source data 1.** Viable cell count of Vc in mouse intestine with and without Pa pre-colonization using *vpsL* mutant with and without *vpsL* complementation plasmid.

---

with our in vitro results, while host colonization was significantly higher for WT Vc coinfecting with Pa than without Pa (**Figure 2C**),  $\Delta rbmA$  mutants did not show any increase in host colonization when coinfecting with Pa, and  $\Delta rbmC \Delta bap1$  mutants demonstrated increased colonization with Pa but less colonization compared with WT Vc co-infection with Pa (**Figure 7B**). These results indicate that the ability of Vc to form a structurally intact biofilm is important for the enhancement of colonization facilitated by the presence of Pa.

## Discussion

Evidence that the composition of the gut microbiota influences the clinical outcomes of enteric infections in humans is accumulating (**Ubeda et al., 2017; Weil et al., 2019**). Several studies have identified commensal species and underlying colonization resistance mechanisms that could be protective against Vc infection. While these studies suggest that microbiota species reduce Vc virulence through various mechanisms during the early stages of infection (**Alavi et al., 2020; Hsiao et al., 2014; You et al., 2019**), the precise role of these colonization resistance mechanisms in impacting susceptibility to cholera in humans has only begun to be appreciated. For instance, a gut bacterium in the genus *Blautia* was recently found to encode functions that confer colonization resistance (e.g., bile salt hydrolase) to Vc infection (**Alavi et al., 2020**). Consistent with this finding, our previous stool microbiome study also independently identified that a species in the genus *Blautia* is correlated with decreased susceptibility to Vc infection (**Levade et al., 2020; Midani et al., 2018**).

While previous studies have identified microbiota-associated mechanisms that are protective against Vc infection, examples of interactions between Vc and a human-associated microbiota species that increases Vc pathogenicity are scarce. Although *Escherichia coli* and Vc are believed to reside in different intestinal niches, one previous study showed that an atypical *E. coli* isolated from a mouse that does not ferment lactose can increase the virulence of a quorum-sensing (QS)-defective Vc strain N16961 (**Yoon et al., 2016**). How QS-proficient Vc strains, which are prevalent among toxigenic clinical isolates (**Wang et al., 2011**), respond to *E. coli* in the human gut remains to be studied. In contrast, a recent study showed that *E. coli* motility facilitates aggregation of these two organisms in a dual-species biofilm, but there was no impact of such aggregation on Vc intestinal colonization (**Wang et al., 2021**). Indeed, coaggregation between Vc and other microbiota species has been observed (**Toh et al., 2019**), but these associations are not known to have a direct influence on Vc pathogenicity. This is consistent with our prior human studies in which *E. coli* species were present in the gut microbiota of persons during active Vc infection, but these were not correlated with active Vc infection (**Midani et al., 2018**). Our findings highlight the importance of coupling mechanistic studies (in vitro and animal models) with human microbiome data analysis to pinpoint the relevant species and interactions involved in enteric infections.

Here, we show that the presence of a human gut microbe Pa promotes Vc host colonization, which is consistent with our prior human study in which Pa was more likely to be present in persons infected with Vc. This raises the possibility that uncharacterized interactions between Vc and members of the gut microbiota may exacerbate Vc virulence and contribute to increased morbidity. While our previous study showed that Vc has a better growth yield in the conditioned medium (CM) harvested from stationary culture of Pa than in the CM harvested from stationary culture Vc, the growth yield of Vc in the CM harvested from stationary culture of Pa does not reach as high as Vc in fresh medium (**Midani**



*et al., 2018*). These results suggest that *Pa* does not actively secrete any molecules that enhance *Vc* growth. Most likely, the limited growth yield increase of *Vc* in the CM harvested from *Pa* is due to the presence of a trace amount of nutrients that have been exhausted in the CM harvested from *Vc*. In contrast, this study establishes a plausible mechanism used by *Pa*, and perhaps other gut microbes, to increase the virulence of *Vc* through induction of biofilm formation, a physiological state in which *Vc* is known to increase expression of other virulence factors critical for human infection and disease (*Tamayo et al., 2010; Gallego-Hernandez et al., 2020*). *Vc* biofilms have also been demonstrated to deform and even damage tissue-engineered soft epithelia mimicking the host tissue (*Cont et al., 2020*), suggesting that in vivo-formed biofilm structures could negatively impact host gut physiology.

While VPS and other biofilm components are not usually considered critical host colonization factors, we found that these macromolecular structures were essential for the enhancement of *Vc* host colonization induced by *Pa*. Whether these components mediate other *Vc*-gut microbe interaction has not been studied. Interestingly, many gut microbes appear to exist in the form of mixed-species biofilms on mucosal surfaces (*Sadiq et al., 2021*), suggesting that microbiota-induced biofilm enhancement could play a major role in modulating virulence of other pathogens. Many structural components, regulatory factors, and signaling transduction pathways that control biofilm formation in *Vc* have been well characterized (*Teschler et al., 2015*), and these factors could be targeted for manipulation by other gut microbes that modulate *Vc* virulence. For example, 3,5-dimethylpyrazin-2-ol (DPO) was recently discovered as a new class of *Vc* QS autoinducer that binds to the transcription factor VqmA to activate expression of *vqmR*, which encodes a small regulatory RNA that downregulates *Vc* biofilm formation. The VqmA-VqmR system can be activated both in vitro by *E. coli* and in vivo by *B. obeum* (*Hsiao et al., 2014; Papenfort et al., 2017*), and results in suppression of biofilm formation. Interestingly, *Pa* demonstrates the opposite tendency by promoting *Vc* biofilm formation, with implications for the enhancement of *Vc* colonization, in contrast to other commensal bacteria.

Many aspects of the *Vc/Pa* interaction are still unclear. What is the selective advantage that fosters the formation of dual-species biofilm? Investigation of the structure–function relationship in other multispecies biofilms, such as dental biofilms, demonstrates a coordinated organization of each species that allows for optimal nutrient and oxygen usage, as well as mechanical stability (*Christensen et al., 2002; Mark Welch et al., 2016*). While we did not observe any growth yield enhancement in the planktonic phase of the co-culture, there was a significant increase of *Vc* and *Pa* abundance in the co-culture pellicle at the air–liquid interface. Thus, a possible driving force of this interaction could be the optimization of nutrient sharing and distribution, or removal of toxic metabolites accumulated during growth. Biofilm formation also changes the biophysical properties of the microbial community that could facilitate host adhesion (*Jiang et al., 2021*). The exact mechanism used by these two species to detect and coordinate with each other remains unclear. Secreted small molecules produced by *Pa* do not appear to impact *Vc* as evidenced by our prior studies in which *Vc* cultured in *Pa* spent-cell supernatant did not result in increased biofilm formation (*Midani et al., 2018*). Therefore, we surmised that the close physical association between *Vc* and *Pa* cells in space in the co-culture pellicles is required for the enhanced biofilm formation. This hypothesis is supported by our microscopy analysis. The *Vc*–*Pa* interaction has two reciprocal aspects: first, *Pa* activates the production of VPS in *Vc* cells, leading to enhanced pellicle formation. Future characterizations of *Pa* could potentially elucidate the underlying molecular mechanism of this effect *Pa* has on *Vc*. Second, in order to be integrated into the pellicle structure, *Pa* cells seem to physically adhere to *Vc* cells or alternatively to the extracellular matrix that *Vc* cells secrete. Future biochemical and biophysical studies to investigate this relationship may provide new insights about the interactions between *Pa* and *Vc* biofilm, and about pathogen–gut microbe interactions in general. Other members of the *Paracoccus* genus are known to form biofilms and encode adhesins to facilitate surface attachment (*Yoshida et al., 2017; Srinandan et al., 2010*), and the potential role of these adhesins in facilitating interaction with *Vc* remains to be studied.

In addition to VPS, the main structural component of *Vc* biofilms, we have shown that matrix proteins, including RbmA, Bap1, and RbmC, are also critical for the enhancement of *Vc* biofilm by *Pa* in the neonatal mouse colonization model. Specifically, we showed that cell–cell adhesion, conferred by RbmA, is more important than cell–surface adhesion conferred by RbmC/Bap1. Previous work established that RbmA is responsible for maintaining dense, structurally robust biofilms (*Berk et al., 2012; Absalon et al., 2011; Fong et al., 2017; Yan et al., 2016*). Therefore, we contemplate that the  $\Delta$ *rbmA* mutant biofilm may be mechanically impaired and become destroyed in the gut environment

by physical forces such as peristaltic flow, food particle collision, and others. Likewise, such physical forces could impede biofilm colonization when biofilm adhesins are absent, which explains the slight defect in colonization of the  $\Delta rbmC\Delta bap1$  mutant. Indeed, recently Vc cells have been visualized in the mouse gut and the biofilm population has been shown to be located primarily at the tip of the villi, where fluid shear is strongest (Gallego-Hernandez et al., 2020). These relationships may be further revealed by additional imaging of the distribution of the Vc and Pa cells and potentially other commensal bacteria in the new mouse model presented here.

In conclusion, we describe a novel interaction between Vc and a gut microbe found in high abundance in Vc-infected persons that leads to a significant change in Vc biofilm behaviors, as well as an increase in the virulence of the pathogen. Our findings are also consistent with other observations that rare gut microbial species can have significant impacts on microbial ecosystems (Jousset et al., 2017). This study adds to the growing number of pathogen–gut microbial species interactions that may impact outcomes in human diseases.

## Materials and methods

### Prior published study sample collection and analysis

In a prior study, we enrolled household contacts of persons hospitalized with cholera at the International Centre for Diarrheal Disease Research, Bangladesh (icddr,b; Midani et al., 2018). Briefly, in this previously published study, household contacts were followed prospectively with rectal swab sampling, 30 days of clinical symptom report, and vibriocidal titer measurements, and 16S rRNA sequencing was performed on rectal swab sampling from the day of enrollment in the study (Midani et al., 2018). Persons with evidence of Vc infection at the time of enrollment in the study were compared to those who did not have evidence of infection in a model to detect gut microbes that were differentially abundant during Vc infection (Midani et al., 2018). Vc infection was defined as Vc DNA identified on 16S rRNA sequencing or a positive Vc stool culture. In this previously published study, we used a machine learning method called a support vector machine (SVM), which utilizes patterns of OTU relative abundance to detect OTUs associated with infected compared to uninfected persons. This SVM was used with a recursive feature elimination algorithm that simplifies models and increases accuracy of the identification of differentially associated OTUs by removing uninformative bacterial taxa (Midani et al., 2018). For this study, we reexamined the microbiome data from household contacts at the time of enrollment to quantify the abundance of 16S rRNA reads that mapped to Pa OTUs between uninfected study participants and infected participants.

### Strains and culture conditions

All Vc strains used in this study are streptomycin-resistant derivatives of C6706, a 1991 El Tor O1 clinical isolate from Peru (Thelin and Taylor, 1996). As *luxO* mutations are readily isolated in this strain (Jung et al., 2015; Stutzmann and Blokesch, 2016), DNA sequencing or cell-density-dependent  $P_{qrr4}$ -*lux* reporter assay (Jung et al., 2015) was performed to confirm our strains carry a functional WT allele of *luxO*. The in-frame  $\Delta vpsL$  deletion mutants used in various assays were previously described (Waters et al., 2008). The  $\Delta rbmA$  and  $\Delta rbmC\Delta bap1$  mutants were constructed by allelic exchange (Skorupski and Taylor, 1996) using specific suicide vectors described before (Nadell et al., 2015; Yan et al., 2016). Vc strains used for microscopy experiments,  $\Delta vc1807::P_{tac}-mNeonGreen$ ,  $\Delta vc1807::P_{tac}-SCFP3A-spec^R$ , and  $\Delta vc1807::P_{tac}-SCFP3A-spec^R \Delta LacZ::P_{vpsL}-mNeonGreen$ , were constructed using natural transformation as previous described (Dalia et al., 2014). For *vpsL* complementation, the reading frame of *vpsL* was first amplified by PCR using Phusion DNA polymerase, C6706 genomic DNA, and primers gataacaatttcacaatgaaggaaaaagcagaatacgcattac and gaattctgttctgttaatacgcgttttccaacaatcctttg. Vector pMMB67eh was linearized by PCR using primers tgtgaaattgttatccgctc and caggaaacagaattcgag. Gibson assembly was used to fuse the two fragments together. The resulting plasmid was transformed into DH5 $\alpha$  and confirmed by sequencing. This plasmid was introduced into Vc by triparental mating with a helper plasmid pRK2013. The Pa used in our experiments is a Strep<sup>R</sup> isolate derived from the ATCC-type strain (ATCC #49632). Vc and Pa overnight cultures were grown with aeration in LB at 30°C. Heat-killed strains were incubated at 60°C for 2 hr prior to experimentation. Unless specified, media were supplemented with streptomycin (Sm, 100  $\mu$ g/mL) and chloramphenicol (Cm, 10  $\mu$ g/mL) when appropriate.

## Animal studies

For establishing colonization of the microbiota species, 3-day-old suckling CD-1 mice (Charles River Laboratories) were fasted for 1 hr, then orally dosed with *Pa* at a concentration of  $10^7$  CFU using 30-gauge plastic tubing, after which the animals were placed with a lactating dam for 10–12 hr and monitored in accordance with the regulations of Tufts Comparative Medicine Services. This inoculation scheme was followed an additional three times at 12, 24, and 36 hr. 12 hr after the last inoculation (i.e., 48 hr after the first inoculation), mice were infected with  $10^6$  CFU of *Vc*, WT C6706 or mutant strain, or LB as a vehicle control in a gavage volume of 50  $\mu$ L to evaluate the effect of *Pa* pre-colonization on *Vc* host colonization. At 18–24 hr post infection, animals were sacrificed, and small intestine tissue samples were collected and homogenized for CFU enumeration. WT *Vc* is *lac*<sup>+</sup> and appears blue on medium containing X-gal while *Pa* appears white on the same medium. For co-infection experiments, cultures of *Vc* and *Pa* strains were mixed in a 1:1 ratio and mice were orally dosed with a final bacterial count of  $10^6$  CFU. Mice were sacrificed 20–24 hr post infection, and small intestine samples were processed as outlined above to evaluate the colonization efficiency of both species.

## Ethics statement

All animal experiments were performed at and in accordance with the rules of the Tufts Comparative Medicine Services (CMS), following the guidelines of the American Veterinary Medical Association (AVMA), as well as the Guide for the Care and Use of Laboratory Animals of the National Institutes of Health. All procedures were performed with approval of the Tufts University CMS (protocol# B 2018-99 and #B2021-81). Euthanasia was performed in accordance with the guidelines provided by the AVMA and was approved by the Tufts CMS. The previously published study from which **Figure 1** is derived (**Midani et al., 2018**) received approval from the Ethical Review Committee at the icddr,b and the institutional review boards of Massachusetts General Hospital and the University of Washington, and in that study participants or their guardians provided written informed consent.

## Pellicle composition analysis

To assess pellicle composition, overnight cultures of *Vc* and *Pa* were inoculated into glass culture tubes (18 × 150 mm) containing 2 mL LB media in a ratio of 1:10 *Vc* ( $10^6$ ) to *Pa* ( $10^7$ ) CFU, and co-cultures were allowed to grow statically at room temperature for 3 days. Following static growth, floating pellicles were carefully transferred into sterile 1.5 mL Eppendorf tubes containing 1 mL LB, and samples were gently spun down to wash away any planktonic bacteria. Planktonic cells were removed, and cell pellets of pellicle samples were resuspended in 1 mL of fresh LB media. All samples, including supernatant from the pellicle wash step, were serially diluted and plated on Sm/X-Gal media to differentiate *Vc* (blue) and *Pa* (white) colonies.

## Crystal violet biomass assays

CV biofilm assays were performed as described previously in 96-well flat-bottom clear, tissue-culture-treated polystyrene microplates (Thermo Fisher; **O'Toole, 2011**). In each well, *Vc* ( $10^6$  CFUs) and/or *Pa* ( $10^6$  or  $10^7$  CFUs) were inoculated into 200  $\mu$ L of medium. Plates were then sealed using a gas-permeable sealing film (BrandTech) and incubated at 37°C. Planktonic culture was removed after 24 hr of incubation, and plates were washed with distilled water once. Attached biofilms were stained with 0.1% CV at room temperature for 15–20 min. The amount of biomass adhered to the sides of each well was quantified by dissolving the CV in 95% ethanol, and the absorbance of the resulting solution was measured at 550 nm using a plate reader.

## Microscopy

Liquid LB culture of *Vc*, *Pa*, and co-cultures (*Vc:Pa* = 1:10) were prepared according to the procedures described above. To image pellicles, we used a modified literature procedure (**Fiebig, 2019**). Monocultures and co-culture pellicles were first prepared following the procedure described above, except that 3 mL of the culture was incubated in a 5 mL culture tube. After 3 days of incubation at room temperature, the pellicles were carefully picked up by the large end of a 200  $\mu$ L pipette tip, transferred to a coverslip (22 × 60 mm, no. 1.5), and immediately covered with another square coverslip to prevent drying. The LB medium contained 4  $\mu$ g/mL FM 4-64 stain (Thermo Fisher) to stain all cells. To stain VPS, the LB medium additionally contained 4  $\mu$ g/mL of WGA conjugated to Oregon

Green (Thermo Fisher). The stained biofilms were imaged with a Nikon-W1 confocal microscope using  $\times 60$  water objective (numerical aperture = 1.20). The imaging window was  $222 \times 222 \mu\text{m}^2$ . For large-scale view, a  $5 \times 5$  tiling was performed. For zoom-in view, the z-step size was  $0.5 \mu\text{m}$  and the pixel size was 108 nm. For large-scale view, the z-step size was  $1 \mu\text{m}$  and the pixel size was 216 nm. The mNeonGreen (or SCFP3A) expressed by Vc was imaged at 488 nm (or 445 nm) excitation, FM 4-64 at 561 nm, and WGA-Oregon Green at 488 nm with the corresponding filters. All presented images are raw images processed from Nikon Element software.

### Quantitative-real-time PCR (qRT-PCR) for Vc virulence factors

Liquid LB culture of Vc, Pa, and co-cultures (Vc:Pa = 1:10) were prepared according to the procedures described above. Samples were inoculated and then incubated statically for 72 hr at room temperature. To measure the relative transcript levels of *vpsL*, *ctxA*, and *tcpA* at the air-liquid interface, 500  $\mu\text{L}$  of liquid culture at the surface of the culture and any present pellicle were extracted at 24, 48, and 72 hr. Samples were treated with TRIzol LS (Invitrogen) and RNA was extracted using chloroform (Fisher Chemical), isopropanol (Fisher Chemical), and ethanol (Fisher Chemical). Extracted RNA was treated with TURBO DNase (Invitrogen) to remove DNA. Integrity and purity were assessed using NanoDrop (ND-1000, Thermo Fisher). cDNA synthesis was performed on 1  $\mu\text{g}$  of RNA using High Capacity cDNA reverse transcriptase (Applied Biosystems) according to the manufacturer's protocol. Resulting cDNA was diluted 1:2, and RT-PCR was performed to measure CtxA, TcpA, and VpsL expression. The primers used were (CtxA-F) 5'-TTGGAGCATTCCCACAACCC-3', (CtxA-R) 5'-GCTCCAGCAGCAGATGGTTA-3' – amplicon 109 bp (Zhao et al., 2018), (TcpA-F) 5'-CGCTGAGACCACACCCATA-3', (TcpA-R) 5'-GAAGAAGTTTGTAAGAAGAACACG-3' – amplicon 103 bp (Fykse et al., 2007), (VpsL-R) 5'-CATTCTGTCGAACATCGCTGG-3', (VpsL-F) 5'-GTAGCGATTCACTATGGTGCGA-3' – amplicon 130 bp, (groEL-F) 5'-ATGATGTTGCCACGCTAGA-3', and (groEL-R) 5'-GGTTATCGCTGCGGTAGAAG-3' – amplicon 117 bp (Fykse et al., 2007). GroEL was used for housekeeping gene. Real-time PCR was performed using SYBR green (Invitrogen) with 0.3  $\mu\text{M}$  of specific primer sets and 2  $\mu\text{L}$  of cDNA sample. PCR amplification was conducted on the StepOne RT-PCR System (Applied Biosystems) with the following conditions: 95°C for 5 min, 40 cycles of 95°C for 5 s, 58°C for 10 s, and 72°C for 15 s, and a final melting temperature analysis of PCR products. Each qRT-PCR run included a no-template and water negative control. Each sample was performed in duplicate. The  $\Delta\Delta\text{CT}$  method was used to calculate fold change in expression levels (Livak and Schmittgen, 2001).

### Statistics

All statistical analyses were performed on GraphPad Prism v9.2 (GraphPad Software, San Diego, CA). Error bars in the figures depict the median with a 95% confidence interval as indicated. Based on the experimental design, either standard *t*-test or Mann-Whitney test was used to compare treatment groups as indicated in each figure legend.

### Acknowledgements

We thank members of the Ng and Weil Labs for helpful discussions. We acknowledge Dr. Andrew Bridges for sharing the *vpsL* reporter strain, Dr. Aretha Fiebig for suggestions on imaging pellicles, and Dr. Ed Ryan for his assistance in reviewing the manuscript. AAW and W-LN received support from a Rozan Award from Tufts University School of Medicine for this project. AAW was supported by AI123494 and W-LN was supported by AI121337 from the National Institute of Allergy and Infectious Diseases (NIAID). JY was supported by DP2GM146253 from the National Institute of General Medical Sciences (NIGMS). JY holds a Career Award at the Scientific Interface from the Burroughs Wellcome Fund (1015763.02). ARS was supported by the Tufts Post-Baccalaureate Research Education (PREP) Program (R25 GM066567).

## Additional information

### Funding


Funder	Grant reference number	Author
National Institutes of Health	AI121337	Wai-Leung Ng
National Institutes of Health	AI123494	Ana A Weil
National Institutes of Health	DP2GM146253	Jing Yan
National Institutes of Health	R25 GM066567	Abigail Rivera Seda
Burroughs Wellcome Fund	1015763.02	Jing Yan

The funders had no role in study design, data collection and interpretation, or the decision to submit the work for publication.

### Author contributions

Kelsey Barrasso, Conceptualization, Formal analysis, Investigation, Methodology, Validation, Writing – original draft, Writing – review and editing; Denise Chac, Formal analysis, Investigation, Methodology, Validation, Writing – review and editing; Meti D Debela, Anjali Steenhaut, Abigail Rivera Seda, Chelsea N Dunmire, Investigation; Catherine Geigel, Conceptualization, Formal analysis, Investigation, Writing – review and editing; Jason B Harris, Firdausi Qadri, Project administration, Resources; Regina C Larocque, Resources; Firas S Midani, Data curation, Formal analysis, Software; Jing Yan, Conceptualization, Formal analysis, Investigation, Methodology, Resources, Supervision, Writing – original draft, Writing – review and editing; Ana A Weil, Wai-Leung Ng, Conceptualization, Formal analysis, Funding acquisition, Investigation, Methodology, Project administration, Supervision, Writing – original draft, Writing – review and editing

### Author ORCIDs

Firas S Midani  <http://orcid.org/0000-0002-2473-7758>  
 Ana A Weil  <http://orcid.org/0000-0002-6170-4306>  
 Wai-Leung Ng  <http://orcid.org/0000-0002-8966-6604>

### Ethics

The previously published study from which Figure 1 is derived from ref (7) received approval from the Ethical Review Committee at the icddr,b and the institutional review boards of Massachusetts General Hospital and the University of Washington. Participants or their guardians provided written informed consent.

All animal experiments were performed at and in accordance with the rules of the Tufts Comparative Medicine Services (CMS), following the guidelines of the American Veterinary Medical Association (AVMA) as well as the Guide for the Care and Use of Laboratory Animals of the National Institutes of Health. All procedures were performed with approval of the Tufts University CMS (Protocol# B 2018-99). Euthanasia was performed in accordance with guidelines provided by the AVMA and was approved by the Tufts CMS.

### Decision letter and Author response

Decision letter <https://doi.org/10.7554/eLife.73010.sa1>

Author response <https://doi.org/10.7554/eLife.73010.sa2>

## Additional files

### Supplementary files

- Supplementary file 1. Raw and normalised counts of *Pa* and *Vc*. (a) Operational taxonomic unit raw and normalized abundance of *Vibrio cholerae* (*Vc*) in *Paracoccus aminovorans* (*Pa*) colonized and *Pa* noncolonized study participants with *Vc* infection. (b) Raw and normalized abundance of total, *Pa*,



and Vc operational taxonomic units in all study participants.

- Transparent reporting form

### Data availability

All data generated or analysed during this study are included in the manuscript and supporting file; Source Data files have been provided for Figures 1-3, 5, 7.

The following previously published dataset was used:

Author(s)	Year	Dataset title	Dataset URL	Database and Identifier
Midani FS, Weil AA, Chowdhury F, Begum YA, Khan AI, Debela MD, Durand HK, Reese AT, Nimmagadda SN, Silverman JD, Ellis CN, Ryan ET, Calderwood SB, Harris JB, Qadri F, David LA, LaRocque RC	2018	Human Gut Microbiota Predicts Susceptibility to <i>Vibrio cholerae</i> Infection	<a href="https://www.ebi.ac.uk/ena/browser/view/PRJEB17860">https://www.ebi.ac.uk/ena/browser/view/PRJEB17860</a>	European Nucleotide Archive accession number, PRJEB17860

## References

- Absalon C**, Van Dellen K, Watnick PI. 2011. A communal bacterial adhesin anchors biofilm and bystander cells to surfaces. *PLOS Pathogens* **7**:e1002210. DOI: <https://doi.org/10.1371/journal.ppat.1002210>
- Alavi S**, Mitchell JD, Cho JY, Liu R, Macbeth JC, Hsiao A. 2020. Interpersonal Gut Microbiome Variation Drives Susceptibility and Resistance to Cholera Infection. *Cell* **181**:1533–1546. DOI: <https://doi.org/10.1016/j.cell.2020.05.036>, PMID: 32631492
- Berk V**, Fong JCN, Dempsey GT, Develioglu ON, Zhuang X, Liphardt J, Yildiz FH, Chu S. 2012. Molecular Architecture and Assembly Principles of *Vibrio cholerae* Biofilms. *Science* **337**:236–239. DOI: <https://doi.org/10.1126/science.1222981>, PMID: 22798614
- Camacho A**, Bouhenia M, Alyusfi R, Alkohani A, Naji MAM, de Radiguès X, Abubakar AM, Almoalmi A, Seguin C, Sagrado MJ, Poncin M, McRae M, Musoke M, Rakesh A, Porten K, Haskew C, Atkins KE, Eggo RM, Azman AS, Broekhuijsen M, et al. 2018. Cholera epidemic in Yemen, 2016–18: an analysis of surveillance data. *The Lancet. Global Health* **6**:e680–e690. DOI: [https://doi.org/10.1016/S2214-109X\(18\)30230-4](https://doi.org/10.1016/S2214-109X(18)30230-4), PMID: 29731398
- Christensen BB**, Haagensen JAJ, Heydorn A, Molin S. 2002. Metabolic Commensalism and Competition in a Two-Species Microbial Consortium. *Applied and Environmental Microbiology* **68**:2495–2502. DOI: <https://doi.org/10.1128/AEM.68.5.2495-2502.2002>, PMID: 11976126
- Cont A**, Rossy T, Al-Mayyah Z, Persat A. 2020. Biofilms deform soft surfaces and disrupt epithelia. *eLife* **9**:e56533. DOI: <https://doi.org/10.7554/eLife.56533>, PMID: 33025904
- Dalia AB**, McDonough E, Camilli A. 2014. Multiplex genome editing by natural transformation. *PNAS* **111**:8937–8942. DOI: <https://doi.org/10.1073/pnas.1406478111>, PMID: 24889608
- David LA**, Weil A, Ryan ET, Calderwood SB, Harris JB, Chowdhury F, Begum Y, Qadri F, LaRocque RC, Turnbaugh PJ. 2015. Gut microbial succession follows acute secretory diarrhea in humans. *MBio* **6**:e00381-15. DOI: <https://doi.org/10.1128/mBio.00381-15>, PMID: 25991682
- DiRita VJ**, Neely M, Taylor RK, Bruss PM. 1996. Differential expression of the ToxR regulon in classical and E1 Tor biotypes of *Vibrio cholerae* is due to biotype-specific control over toxT expression. *PNAS* **93**:7991–7995. DOI: <https://doi.org/10.1073/pnas.93.15.7991>, PMID: 8755590
- Fiebig A**. 2019. Role of Caulobacter Cell Surface Structures in Colonization of the Air-Liquid Interface. *Journal of Bacteriology* **201**:e00064-19. DOI: <https://doi.org/10.1128/JB.00064-19>, PMID: 31010900
- Fong J**, Karplus K, Schoolnik GK, Yildiz FH. 2006. Identification and Characterization of RbmA, a Novel Protein Required for the Development of Rugose Colony Morphology and Biofilm Structure in *Vibrio cholerae*. *Journal of Bacteriology* **188**:1049–1059. DOI: <https://doi.org/10.1128/JB.188.3.1049-1059.2006>, PMID: 16428409
- Fong J**, Yildiz FH. 2007. The rbmBCDEF Gene Cluster Modulates Development of Rugose Colony Morphology and Biofilm Formation in *Vibrio cholerae*. *Journal of Bacteriology* **189**:2319–2330. DOI: <https://doi.org/10.1128/JB.01569-06>, PMID: 17220218
- Fong J**, Syed KA, Klose KE, Yildiz FH. 2010. Role of *Vibrio* polysaccharide (VPS) genes in VPS production, biofilm formation and *Vibrio cholerae* pathogenesis. *Microbiology* **156**:2757–2769. DOI: <https://doi.org/10.1099/mic.0.040196-0>, PMID: 20466768
- Fong JC**, Rogers A, Michael AK, Parsley NC, Cornell W-C, Lin Y-C, Singh PK, Hartmann R, Drescher K, Vinogradov E, Dietrich LE, Partch CL, Yildiz FH. 2017. Structural dynamics of RbmA governs plasticity of *Vibrio cholerae* biofilms. *eLife* **6**:e26163. DOI: <https://doi.org/10.7554/eLife.26163>, PMID: 28762945

- Freter R. 1955. The fatal enteric cholera infection in the guinea pig, achieved by inhibition of normal enteric flora. *The Journal of Infectious Diseases* **97**:57–65. DOI: <https://doi.org/10.1093/infdis/97.1.57>, PMID: 13242854
- Fykse EM, Skogan G, Davies W, Olsen JS, Blatny JM. 2007. Detection of *Vibrio cholerae* by real-time nucleic acid sequence-based amplification. *Applied and Environmental Microbiology* **73**:1457–1466. DOI: <https://doi.org/10.1128/AEM.01635-06>, PMID: 17220262
- Gallego-Hernandez AL, DePas WH, Park JH, Teschler JK, Hartmann R, Jeckel H, Drescher K, Beyhan S, Newman DK, Yildiz FH. 2020. Upregulation of virulence genes promotes *Vibrio cholerae* biofilm hyperinfectivity. *PNAS* **117**:11010–11017. DOI: <https://doi.org/10.1073/pnas.1916571117>, PMID: 32355001
- Hsiao A, Ahmed AMS, Subramanian S, Griffin NW, Drewry LL, Petri WA Jr, Haque R, Ahmed T, Gordon JI. 2014. Members of the human gut microbiota involved in recovery from *Vibrio cholerae* infection. *Nature* **515**:423–426. DOI: <https://doi.org/10.1038/nature13738>, PMID: 25231861
- Iwanaga M, Yamamoto K, Higa N, Ichinose Y, Nakasone N, Tanabe M. 1986. Culture Conditions for Stimulating Cholera Toxin Production by *Vibrio cholerae* O1 El Tor. *Microbiology and Immunology* **30**:1075–1083. DOI: <https://doi.org/10.1111/j.1348-0421.1986.tb03037.x>, PMID: 3543624
- Jiang Z, Nero T, Mukherjee S, Olson R, Yan J. 2021. Searching for the Secret of Stickiness: How Biofilms Adhere to Surfaces. *Frontiers in Microbiology* **12**:686793. DOI: <https://doi.org/10.3389/fmicb.2021.686793>, PMID: 34305846
- Jousset A, Bienhold C, Chatzinotas A, Gallien L, Gobet A, Kurm V, Küsel K, Rillig MC, Rivett DW, Salles JF, van der Heijden MGA, Youssef NH, Zhang X, Wei Z, Hol WHG. 2017. Where less may be more: how the rare biosphere pulls ecosystems strings. *The ISME Journal* **11**:853–862. DOI: <https://doi.org/10.1038/ismej.2016.174>, PMID: 28072420
- Jung SA, Chapman CA, Ng WL. 2015. Quadruple quorum-sensing inputs control *Vibrio cholerae* virulence and maintain system robustness. *PLOS Pathogens* **11**:e1004837. DOI: <https://doi.org/10.1371/journal.ppat.1004837>, PMID: 25874462
- Kim Y-G, Sakamoto K, Seo S-U, Pickard JM, Gilliland MG, Pudlo NA, Hoostal M, Li X, Wang TD, Feehley T, Stefka AT, Schmidt TM, Martens EC, Fukuda S, Inohara N, Nagler CR, Núñez G. 2017. Neonatal acquisition of *Clostridia* species protects against colonization by bacterial pathogens. *Science (New York, N.Y.)* **356**:315–319. DOI: <https://doi.org/10.1126/science.aag2029>, PMID: 28428425
- Klose KE. 2000. The suckling mouse model of cholera. *Trends in Microbiology* **8**:189–191. DOI: [https://doi.org/10.1016/s0966-842x\(00\)01721-2](https://doi.org/10.1016/s0966-842x(00)01721-2), PMID: 10754579
- Levade I, Saber MM, Midani F, Chowdhury F, Khan AI, Begum YA, Ryan ET, David LA, Calderwood SB, Harris JB, LaRocque RC, Qadri F, Shapiro BJ, Weil AA. 2020. Predicting *Vibrio cholerae* Infection and Disease Severity Using Metagenomics in a Prospective Cohort Study. *The Journal of Infectious Diseases* **223**:342–351. DOI: <https://doi.org/10.1093/infdis/jiaa358>
- Livak KJ, Schmittgen TD. 2001. Analysis of relative gene expression data using real-time quantitative PCR and the 2<sup>-</sup>(Delta Delta C(T)) Method. *Methods (San Diego, Calif.)* **25**:402–408. DOI: <https://doi.org/10.1006/meth.2001.1262>, PMID: 11846609
- Luquero FJ, Rondy M, Boncy J, Munger A, Mekaoui H, Rymshaw E, Page A-L, Toure B, Degail MA, Nicolas S, Grandesso F, Ginsbourger M, Polonsky J, Alberti KP, Terzian M, Olson D, Porten K, Ciglenecki I. 2016. Mortality Rates during Cholera Epidemic, Haiti, 2010–2011. *Emerging Infectious Diseases* **22**:410–416. DOI: <https://doi.org/10.3201/eid2203.141970>, PMID: 26886511
- Mark Welch JL, Rossetti BJ, Rieken CW, Dewhirst FE, Borisy GG. 2016. Biogeography of a human oral microbiome at the micron scale. *PNAS* **113**:E791–E800. DOI: <https://doi.org/10.1073/pnas.1522149113>, PMID: 26811460
- McKenney PT, Pamer EG. 2015. From Hype to Hope: The Gut Microbiota in Enteric Infectious Disease. *Cell* **163**:1326–1332. DOI: <https://doi.org/10.1016/j.cell.2015.11.032>, PMID: 26638069
- Midani FS, Weil AA, Chowdhury F, Begum YA, Khan AI, Debela MD, Durand HK, Reese AT, Nimmagadda SN, Silverman JD, Ellis CN, Ryan ET, Calderwood SB, Harris JB, Qadri F, David LA, LaRocque RC. 2018. Human Gut Microbiota Predicts Susceptibility to *Vibrio cholerae* Infection. *The Journal of Infectious Diseases* **218**:645–653. DOI: <https://doi.org/10.1093/infdis/jiy192>, PMID: 29659916
- Millet YA. 2014. Insights into *Vibrio cholerae* intestinal colonization from monitoring fluorescently labeled bacteria. *PLOS Pathogens* **10**:e1004405. DOI: <https://doi.org/10.1371/journal.ppat.1004405>
- Nadell CD, Drescher K, Wingreen NS, Bassler BL. 2015. Extracellular matrix structure governs invasion resistance in bacterial biofilms. *The ISME Journal* **9**:1700–1709. DOI: <https://doi.org/10.1038/ismej.2014.246>, PMID: 25603396
- Nygren E, Li BL, Holmgren J, Attridge SR. 2009. Establishment of an adult mouse model for direct evaluation of the efficacy of vaccines against *Vibrio cholerae*. *Infection and Immunity* **77**:3475–3484. DOI: <https://doi.org/10.1128/IAI.01197-08>, PMID: 19470748
- O'Toole GA. 2011. Microtiter dish biofilm formation assay. *Journal of Visualized Experiments* **47**:2437. DOI: <https://doi.org/10.3791/2437>, PMID: 21307833
- Papenfort K, Silpe JE, Schramma KR, Cong J-P, Seyedsayamdost MR, Bassler BL. 2017. A *Vibrio cholerae* autoinducer-receptor pair that controls biofilm formation. *Nature Chemical Biology* **13**:551–557. DOI: <https://doi.org/10.1038/nchembio.2336>, PMID: 28319101
- Sadiq FA, Wenwei L, Heyndrickx M, Flint S, Wei C, Jianxin Z, Zhang H. 2021. Synergistic interactions prevail in multispecies biofilms formed by the human gut microbiota on mucin. *FEMS Microbiology Ecology* **97**:fiab096. DOI: <https://doi.org/10.1093/femsec/fiab096>, PMID: 34190973

- Salter SJ**, Cox MJ, Turek EM. 2014. Reagent and laboratory contamination can critically impact sequence-based microbiome analyses. *BMC Biology* **12**:87. DOI: <https://doi.org/10.1186/s12915-014-0087-z>
- Shaner NC**, Lambert GG, Chammas A, Ni Y, Cranfill PJ, Baird MA, Sell BR, Allen JR, Day RN, Israelsson M, Davidson MW, Wang J. 2013. A bright monomeric green fluorescent protein derived from *Branchiostoma lanceolatum*. *Nature Methods* **10**:407–409. DOI: <https://doi.org/10.1038/nmeth.2413>, PMID: 23524392
- Singer JR**, Blosser EG, Zindl CL, Silberger DJ, Conlan S, Laufer VA, DiToro D, Deming C, Kumar R, Morrow CD, Segre JA, Gray MJ, Randolph DA, Weaver CT. 2019. Preventing dysbiosis of the neonatal mouse intestinal microbiome protects against late-onset sepsis. *Nature Medicine* **25**:1772–1782. DOI: <https://doi.org/10.1038/s41591-019-0640-y>, PMID: 31700190
- Skorupski K**, Taylor RK. 1996. Positive selection vectors for allelic exchange. *Gene* **169**:47–52. DOI: [https://doi.org/10.1016/0378-1119\(95\)00793-8](https://doi.org/10.1016/0378-1119(95)00793-8), PMID: 8635748
- Srinandan CS**, Jadav V, Cecilia D, Nerurkar AS. 2010. Nutrients determine the spatial architecture of *Paracoccus* sp. *Biofouling* **26**:449–459. DOI: <https://doi.org/10.1080/08927011003739760>
- Stutzmann S**, Blokesch M. 2016. Circulation of a Quorum-Sensing-Impaired Variant of *Vibrio cholerae* Strain C6706 Masks Important Phenotypes. *MSphere* **1**:e00098-16. DOI: <https://doi.org/10.1128/mSphere.00098-16>, PMID: 27303743
- Tamayo R**, Patimalla B, Camilli A. 2010. Growth in a biofilm induces a hyperinfectious phenotype in *Vibrio cholerae*. *Infection and Immunity* **78**:3560–3569. DOI: <https://doi.org/10.1128/IAI.00048-10>
- Teschler JK**, Zamorano-Sánchez D, Utada AS, Warner CJA, Wong GCL, Lington RG, Yildiz FH. 2015. Living in the matrix: assembly and control of *Vibrio cholerae* biofilms. *Nature Reviews. Microbiology* **13**:255–268. DOI: <https://doi.org/10.1038/nrmicro3433>, PMID: 25895940
- Theilin KH**, Taylor RK. 1996. Toxin-coregulated pilus, but not mannose-sensitive hemagglutinin, is required for colonization by *Vibrio cholerae* O1 El Tor biotype and O139 strains. *Infection and Immunity* **64**:2853–2856. DOI: <https://doi.org/10.1128/iai.64.7.2853-2856.1996>, PMID: 8698524
- Toh YS**, Yeoh SL, Yap IKS, Teh CSJ, Win TT, Thong KL, Chong CW. 2019. Role of coaggregation in the pathogenicity and prolonged colonisation of *Vibrio cholerae*. *Medical Microbiology and Immunology* **208**:793–809. DOI: <https://doi.org/10.1007/s00430-019-00628-3>, PMID: 31263955
- Ubeda C**, Djukovic A, Isaac S. 2017. Roles of the intestinal microbiota in pathogen protection. *Clinical & Translational Immunology* **6**:e128. DOI: <https://doi.org/10.1038/cti.2017.2>, PMID: 28243438
- Urakami T**, Araki H, Oyanagi H, Suzuki KI, Komagata K. 1990. *Paracoccus aminophilus* sp nov and *Paracoccus aminovorans* sp nov, Which Utilize N,N-Dimethylformamide. *International Journal of Systematic Bacteriology* **40**:287–291. DOI: <https://doi.org/10.1099/00207713-40-3-287>, PMID: 2397196
- Wang Y**, Wang H, Cui Z, Chen H, Zhong Z, Kan B, Zhu J. 2011. The Prevalence of Functional Quorum-Sensing Systems in Recently Emerged *Vibrio cholerae* Toxigenic Strains. *Environmental Microbiology Reports* **3**:218–222. DOI: <https://doi.org/10.1111/j.1758-2229.2010.00212.x>, PMID: 21643457
- Wang H**, Li F, Xu L, Byun H, Fan J, Wang M, Li M, Zhu J, Li B. 2021. Contributions of *Escherichia coli* and Its Motility to the Formation of Dual-Species Biofilms with *Vibrio cholerae*. *Applied and Environmental Microbiology* **87**:e0093821. DOI: <https://doi.org/10.1128/AEM.00938-21>, PMID: 34260307
- Waters CM**, Lu W, Rabinowitz JD, Bassler BL. 2008. Quorum sensing controls biofilm formation in *Vibrio cholerae* through modulation of cyclic di-GMP levels and repression of *vpsT*. *Journal of Bacteriology* **190**:2527–2536. DOI: <https://doi.org/10.1128/JB.01756-07>, PMID: 18223081
- Watve S**, Barrasso K, Jung SA, Davis KJ, Hawver LA, Khataoka A, Palaganas RG, Neiditch MB, Perez LJ, Ng WL. 2020. Parallel quorum-sensing system in *Vibrio cholerae* prevents signal interference inside the host. *PLOS Pathogens* **16**:e1008313. DOI: <https://doi.org/10.1371/journal.ppat.1008313>, PMID: 32059031
- Weil AA**, Ryan ET. 2018. Cholera: recent updates. *Current Opinion in Infectious Diseases* **31**:455–461. DOI: <https://doi.org/10.1097/QCO.0000000000000474>, PMID: 30048254
- Weil AA**, Becker RL, Harris JB. 2019. *Vibrio cholerae* at the Intersection of Immunity and the Microbiome. *MSphere* **4**:e00597. DOI: <https://doi.org/10.1128/mSphere.00597-19>, PMID: 31776240
- Yan J**, Sharo AG, Stone HA, Wingreen NS, Bassler BL. 2016. *Vibrio cholerae* biofilm growth program and architecture revealed by single-cell live imaging. *PNAS* **113**:E5337–E5343. DOI: <https://doi.org/10.1073/pnas.1611494113>, PMID: 27555592
- Yatsunenko T**, Rey FE, Manary MJ, Trehan I, Dominguez-Bello MG, Contreras M, Magris M, Hidalgo G, Baldassano RN, Anokhin AP, Heath AC, Warner B, Reeder J, Kuczynski J, Caporaso JG, Lozupone CA, Lauber C, Clemente JC, Knights D, Knight R, et al. 2012. Human gut microbiome viewed across age and geography. *Nature* **486**:222–227. DOI: <https://doi.org/10.1038/nature11053>, PMID: 22699611
- Yildiz FH**, Schoolnik GK. 1999. *Vibrio cholerae* O1 El Tor: identification of a gene cluster required for the rugose colony type, exopolysaccharide production, chlorine resistance, and biofilm formation. *PNAS* **96**:4028–4033. DOI: <https://doi.org/10.1073/pnas.96.7.4028>, PMID: 10097157
- Yildiz F**, Fong J, Sadovskaya I, Grard T, Vinogradov E. 2014. Structural characterization of the extracellular polysaccharide from *Vibrio cholerae* O1 El-Tor. *PLOS ONE* **9**:e86751. DOI: <https://doi.org/10.1371/journal.pone.0086751>, PMID: 24520310
- Yoon MY**, Min KB, Lee K-M, Yoon Y, Kim Y, Oh YT, Lee K, Chun J, Kim B-Y, Yoon S-H, Lee I, Kim CY, Yoon SS. 2016. A single gene of a commensal microbe affects host susceptibility to enteric infection. *Nature Communications* **7**:11606. DOI: <https://doi.org/10.1038/ncomms11606>, PMID: 27173141
- Yoshida K**, Toyofuku M, Obana N, Nomura N. 2017. Biofilm formation by *Paracoccus denitrificans* requires a type I secretion system-dependent adhesin BpA. *FEMS Microbiology Letters* **364**:fnx029. DOI: <https://doi.org/10.1093/femsle/fnx029>, PMID: 28158695

- You JS**, Yong JH, Kim GH, Moon S, Nam KT, Ryu JH, Yoon MY, Yoon SS. 2019. Commensal-derived metabolites govern *Vibrio cholerae* pathogenesis in host intestine. *Microbiome* **7**:132. DOI: <https://doi.org/10.1186/s40168-019-0746-y>, PMID: 31521198
- Zhao W**, Caro F, Robins W, Mekalanos JJ. 2018. Antagonism toward the intestinal microbiota and its effect on *Vibrio cholerae* virulence. *Science (New York, N.Y.)* **359**:210–213. DOI: <https://doi.org/10.1126/science.aap8775>, PMID: 29326272
- Zhu J**, Mekalanos JJ. 2003. Quorum Sensing-Dependent Biofilms Enhance Colonization in *Vibrio cholerae*. *Developmental Cell* **5**:647–656. DOI: [https://doi.org/10.1016/S1534-5807\(03\)00295-8](https://doi.org/10.1016/S1534-5807(03)00295-8), PMID: 14536065